epithelial cell adhesion molecule (EpCAM) and alpha-fetoprotein (AFP), which correlate with distinct gene-expression signatures and prognosis.[8,9] $EpCAM^+$ HCC cells isolated from primary HCC and cell lines show CSC features, including tumorigenicity, invasiveness, and resistance to fluorouracil (5-FU).[10] Similarly, other groups have shown that $CD133^+$, $CD90^+$, and $CD13^+$ HCC cells are also CSCs, and that EpCAM, CD90, and CD133 are the only markers confirmed to enrich CSCs from primary HCCs thus far.[3-5,10]

Although $EpCAM^+$, $CD90^+$, and $CD133^+$ cells show CSC features, such as high tumorigenicity, an invasive nature, and resistance to chemo- and radiation therapy, it remains unclear whether these cells represent an identical HCC population and whether they share similar or distinct characteristics. In this study, we used fluorescent-activated cell sorting (FACS), microarray, and immunohistochemistry (IHC) techniques to investigate the expression patterns of the representative liver CSC markers CD133, CD90, and EpCAM in a total of 340 HCC cases and 7 cases of mesenchymal liver tumors. We further explored gene- and protein-expression patterns as well as tumorigenic capacity of sorted cells isolated from 15 primary HCCs and 7 liver cancer cell lines in an attempt to identify the molecular portraits of each cell type.

Materials and Methods

Clinical Specimens. HCC samples were obtained with informed consent from patients who had undergone radical resection at the Liver Center in Kanazawa University Hospital (Kanazawa, Japan), and tissue acquisition procedures were approved by the ethics committee of Kanazawa University. A total of 102 formalin-fixed and paraffin-embedded HCC samples, obtained from 2001 to 2007, were used for IHC analyses. Fifteen fresh HCC samples were obtained between 2008 and 2012 from surgically resected specimens and an autopsy specimen and were used immediately to prepare single-cell suspensions and xenotransplantation (Table 1). Seven hepatic stromal tumors (three cavernous hemangioma, two hemangioendothelioma, and two angiomyolipoma) were formalin fixed and paraffin embedded and used for IHC analyses.

Table 1. Clinicopathological Characteristics of HCC Cases Used for Xenotransplantation

ID	Age/ Sex	Etiology	Tumor Size (cm)	Histological Grade	AFP (ng/mL)	DCP (IU/mL)
P1	77/M	Alcohol	12.0	Moderate	198	322
P2	61/F	NBNC	11.0	Moderate	12	3,291
P3	66/M	NBNC	2.2	Moderate	13	45
P4	65/M	HCV	4.2	Poor	13,700	25,977
P5	52/M	HBV	6.0	Moderate	29,830	1,177
P6	60/M	HCV	2.7	Poor	249	185
P7	79/F	HBV	4.0	Poor	46,410	384
P8	77/F	NBNC	5.5	Moderate	17,590	562
P9	71/M	Alcohol	7.0	Poor	3,814	607
P10	51/M	HBV	2.2	Well	<10	21
P11	71/M	Alcohol	2.1	Well	<10	11
P12	60/M	HBV	10.8	Poor	323	2,359
P13	66/M	HCV	2.8	Moderate	11	29
P14	71/M	HCV	7.2	Moderate	235,700	375,080
P15	75/M	HBV	5.5	Poor	<10	97

Abbreviation: DCP, des-gamma-carboxy prothrombin.

Additional details of experimental procedures are available in the Supporting Information.

Results

EpCAM, CD133, and CD90 Expression in HCC. We first evaluated the frequencies of three representative CSC markers ($EpCAM^+$, $CD90^+$, and $CD133^+$ cells) in 12 fresh primary HCC cases surgically resected by FACS (representative data shown in Fig. 1A). Clinicopathological characteristics of primary HCC cases are shown in Table 1. We noted that frequency of $EpCAM^+$, $CD90^+$, and $CD133^+$ cells varied between individuals. Abundant $CD90^+$ (7.0%), but almost no $EpCAM^+$, cells (0.06%, comparable to the isotype control) were detected in P2, whereas few $CD90^+$ (0.6%), but abundant $EpCAM^+$, cells (17.5%) were detected in P4. Very small populations of $EpCAM^+$ (0.09%), $CD90^+$ (0.04%), and $CD133^+$ cells (0.05%) were found in P12, but they were almost nonexistent in P8, except for $CD90^+$ cells (0.08%) (Fig. 1A). We further evaluated the expression of EpCAM, CD90, and CD133 in xenografts obtained from surgically resected samples (P13 and P15) and an autopsy sample (P14). As a whole, compared to the isotype control, 7 of 15 HCCs contained definite $EpCAM^+$ cells (46.7%), whereas only 3 HCCs

Address reprint requests to: Taro Yamashita, M.D., Ph.D., Department of General Medicine, Kanazawa University Hospital, 13-1 Takara-Machi, Kanazawa, Ishikawa 920-8641, Japan. E-mail: taroy@m-kanazawa.jp; fax: +81-76-234-4250.

View this article online at wileyonlinelibrary.com.

DOI 10.1002/hep.26168

Potential conflict of interest: Nothing to report.

Additional Supporting Information may be found in the online version of this article.

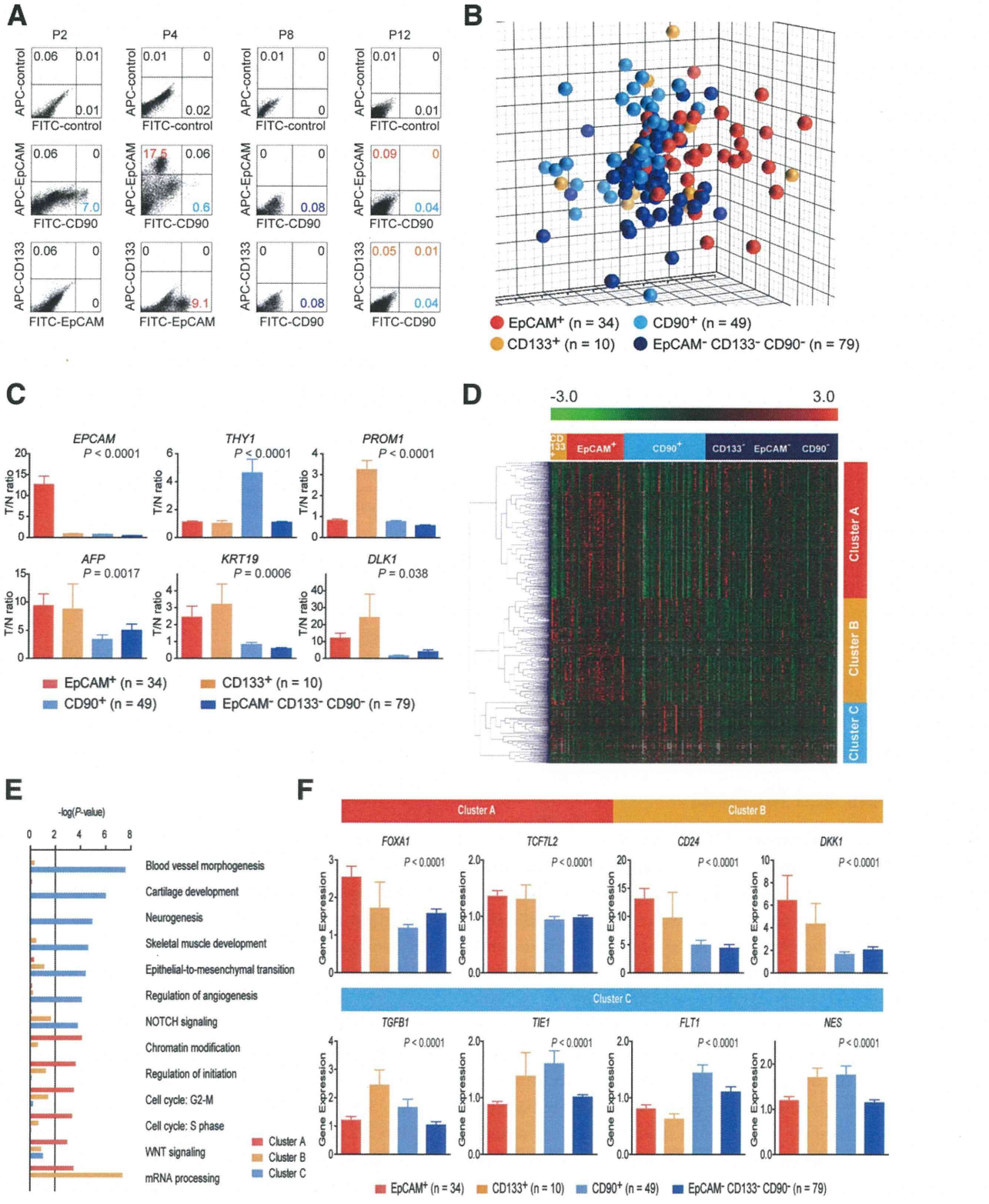

Fig. 1. Gene-expression profiles of CSC marker-positive HCCs. (A) FACS analysis of primary HCCs stained with fluorescent-labeled Abs against EpCAM, CD90, or CD133. (B) Multidimensional scaling analysis of 172 HCC cases characterized by the expression patterns of EpCAM, CD133, and CD90. Red, $EpCAM^+$ $CD90^-$ $CD133^-$ (n = 34); orange, $EpCAM^-$ $CD90^-$ $CD133^+$ (n = 10); light blue, $EpCAM^-$ $CD90^+$ $CD133^-$ (n = 49); blue, $EpCAM^-$ $CD90^-$ $CD133^-$ (n = 79). HCC specimens were clustered in specific groups with statistical significance ($P < 0.001$). (C) Expression patterns of well-known hepatic stem/progenitor markers in each HCC subtype, as analyzed by microarray. Red bar, $EpCAM^+$; orange bar, $CD133^+$; light blue bar, $CD90^+$; blue bar, $EpCAM^-$ $CD90^-$ $CD133^-$. (D) Hierarchical cluster analysis based on 1,561 EpCAM/CD90/CD133-coregulated genes in 172 HCC cases. Each cell in the matrix represents the expression level of a gene in an individual sample. Red and green cells depict high and low expression levels, respectively, as indicated by the scale bar. (E) Pathway analysis of EpCAM/CD90/CD133-coregulated genes. Canonical signaling pathways activated in cluster A (red bar), cluster B (orange bar), or cluster C (light blue bar) with statistical significance ($P < 0.01$) are shown. (F) Expression patterns of representative genes differentially expressed in EpCAM/CD90/CD133 HCC subtypes. Red bar, $EpCAM^+$; orange bar, $CD133^+$; light blue bar, $CD90^+$; blue bar, $EpCAM^-$ $CD133^-$ $CD90^-$.

Table 2. Tumorigenic Capacity of Unsorted, EpCAM$^+$, EpCAM$^-$, CD90$^+$, and CD90$^-$ Cells From Primary HCCs and Xenografts

Sample	CD133 (%)	CD90 (%)	EpCAM (%)	Cell Surface Marker	Number of Cells	Tumor Formation 2M	Tumor Formation 3M
P1	0	3.1	0	Unsorted	1×10^7	0/5	0/5
				CD90$^+$	1×10^5	0/5	0/5
				CD90$^-$	1×10^5	0/5	0/5
P2	0.06	7.0	0.06	Unsorted	1×10^7	0/5	0/5
				CD90$^+$	1×10^5	0/5	0/5
				CD90$^-$	1×10^5	0/5	0/5
P3	0	1.3	0	Unsorted	1×10^6	0/2	0/2
				CD90$^+$	1×10^4	0/4	0/4
				CD90$^-$	1×10^4	0/4	0/4
P4	0	0.6	17.5	Unsorted	1×10^6	3/4	4/4
				EpCAM$^+$	1×10^3	0/3	2/3
					1×10^4	3/4	4/4
					1×10^5	3/3	3/3
				CD90$^+$	1×10^3	0/3	0/3
					1×10^4	0/4	0/4
					1×10^5	0/3	0/3
				EpCAM$^-$ CD90$^-$	1×10^3	0/3	0/3
					1×10^4	0/4	0/4
					1×10^5	0/3	0/3
P5	0	0.8	29.7	Unsorted	1×10^6	0/5	0/5
				EpCAM$^+$	1×10^5	0/5	0/5
				CD90$^+$	1×10^5	0/5	0/5
				EpCAM$^-$ CD90$^-$	1×10^5	0/5	0/5
P6	0	0.7	0	Unsorted	1×10^6	0/2	0/2
				CD90$^+$	1×10^4	0/4	0/4
				CD90$^-$	1×10^4	0/4	0/4
P7	1.38	4.5	4.4	Unsorted	1×10^6	2/2	2/2
				EpCAM$^+$	2×10^2	0/3	0/3
					1×10^3	0/3	1/3
					1×10^4	2/4	4/4
				CD90$^+$	2×10^2	0/3	0/3
					1×10^3	0/3	0/3
					1×10^4	0/4	0/4
				EpCAM$^-$ CD90$^-$	1×10^3	0/3	0/3
					1×10^4	0/3	0/3
					1×10^5	0/4	0/4
P8	0	0.08	0	Unsorted	1×10^5	0/4	0/4
				CD90$^+$	1×10^3	0/3	0/3
				CD90$^-$	1×10^5	0/3	0/3
P9	0	0.26	0	Unsorted	1×10^5	0/4	0/4
				CD90$^+$	1×10^3	0/3	0/3
				CD90$^-$	1×10^5	0/3	0/3
P10	0	0.78	0	Unsorted	1×10^4	0/4	0/4
				CD90$^+$	1×10^3	0/3	0/3
				CD90$^-$	1×10^4	0/3	0/3
P11	0	0.1	1.54	Unsorted	5×10^4	0/2	0/2
				EpCAM$^+$	1×10^3	0/3	0/3
				CD90$^+$	1×10^3	0/3	0/3
				EpCAM$^-$ CD90$^-$	1×10^4	0/3	0/3
P12	0.06	0.05	0.09	Unsorted	1×10^5	0/3	3/3
				CD90$^+$	1×10^3	0/4	1/4
				CD90$^-$	1×10^3	0/4	1/4
					1×10^4	0/3	3/3
P13	0	0.03	67.7	EpCAM$^+$	5×10^5	4/4	NA
					5×10^4	3/3	NA
					5×10^3	3/3	NA
				EpCAM$^-$	5×10^5	0/4	NA
					5×10^4	0/3	NA
					5×10^3	0/3	NA
P14	24.0	0.06	3.1	EpCAM$^+$	5×10^3	4/5	NA
				EpCAM$^-$	5×10^3	2/5	NA
P15	0	2.45	0	CD90$^+$	5×10^4	3/4	NA
					5×10^3	1/3	NA
					5×10^2	1/3	NA
				CD90$^-$	5×10^4	2/4	NA
					5×10^3	1/3	NA
					5×10^2	0/3	NA

NA, not available.

contained definite CD133$^+$ cells (20%) (Table 2). CD90$^+$ cells were detected at variable frequencies in all 15 HCCs analyzed.

To explore the status of these CSC marker-positive cells in HCC in a large cohort, we utilized oligo-DNA microarray data from 238 HCC cases (GEO accession no.: GSE5975) to evaluate the expression of *EPCAM* (encoding EpCAM and CD326), *THY1* (encoding CD90), and *PROM1* (encoding CD133) in whole HCC tissues and nontumor (NT) tissues. Because previous studies demonstrated that CD133$^+$ and CD90$^+$ cells were detected at low frequency (~13.6% by CD133 staining and ~6.2% by CD90 staining) in HCC, but were almost nonexistent in NT liver (4, 5),[4,5] we utilized tumor/nontumor (T/N) gene-expression ratios to detect the existence of marker-positive CSCs in tumor. Accordingly, we showed that a 2-fold cutoff of T/N ratios of *EPCAM* successfully stratifies HCC samples with EpCAM$^+$ liver CSCs.[9,10]

A total of 95 (39.9%), 110 (46.2%), and 31 (13.0%) of the 238 HCC cases were thus regarded as EpCAM$^+$, CD90$^+$, and CD133$^+$ HCCs (T/N ratios: $\geq$2.0), respectively. As observed in the FACS data described above, we detected coexpression of EpCAM and CD90 in 45 HCCs (18.9%), EpCAM and CD133 in five HCCs (2%), CD90 and CD133 in five HCCs (2%), and EpCAM, CD90, and CD133 in 11 HCCs (4.6%). To clarify the characteristics of gene-expression signatures specific to stem cell marker expression status, we selected 172 HCC cases expressing a single CSC marker (34 EpCAM$^+$ CD90$^-$ CD133$^-$, 49 EpCAM$^-$ CD90$^+$ CD133$^-$, and 10 EpCAM$^-$ CD90$^-$ CD133$^+$) or all marker-negative HCCs (79 EpCAM$^-$ CD90$^-$ CD133$^-$). A class-comparison analysis with

univariate F tests and a global permutation test (×10,000) yielded a total of 1,561 differentially expressed genes. Multidimensional scaling (MDS) analysis using this gene set indicated that HCC specimens were clustered in specific groups with statistical significance ($P < 0.001$). Close examination of MDS plots revealed three major HCC subtype clusters: all marker-negative HCCs (blue spheres); EpCAM single-positive HCCs (red spheres); and CD90 single-positive HCCs (light blue spheres). $CD133^+$ HCCs (orange spheres) were rare, relatively scattered, and not clustered (Fig. 1B).

We examined the expression of representative hepatic stem/progenitor cell markers *AFP*, *KRT19*, and *DLK1* in HCCs with regard to the gene-expression status of each CSC marker (Fig. 1C). All three markers were up-regulated in $EpCAM^+$ and $CD133^+$ HCCs, compared with all marker-negative HCCs, consistent with previous findings.[10,11] However, we found no significant overexpression of *AFP*, *KRT19*, and *DLK1* in $CD90^+$ and all marker-negative HCCs.

Hierarchical cluster analyses revealed three main gene clusters that were up-regulated in $EpCAM^+$ HCCs (cluster A, 706 genes), $EpCAM^+$ or $CD133^+$ HCCs (cluster B, 530 genes), and $CD90^+$ or $CD133^+$ HCCs (cluster C, 325 genes) (Fig. 1D). Pathway analysis indicated that the enriched genes in cluster A (red bar) were associated with chromatin modification, cell-cycle regulation, and Wnt/β-catenin signaling (Fig. 1E). Genes associated with messenger RNA processing were enriched in clusters A (red bar) and B (orange bar). Surprisingly, genes in cluster C were significantly associated with pathways involved in blood-vessel morphogenesis, angiogenesis, neurogenesis, and epithelial mesenchymal transition (EMT) (light blue bar). Close examination of genes in each cluster suggested that known hepatic transcription factors (*FOXA1*), Wnt regulators (*TCF7L2* and *DKK1*), and a hepatic stem cell marker (*CD24*) were dominantly up-regulated in $EpCAM^+$ and $CD133^+$ HCCs (Fig. 1F). By contrast, genes associated with blood-vessel morphogenesis (*TIE1* and *FLT1*), EMT (*TGFB1*), and neurogenesis (*NES*) were activated dominantly in $CD90^+$ HCCs and $CD133^+$ HCCs.

$CD90^+$ HCC Cells Share Features With Mesenchymal Vascular Endothelial Cells. Because $CD133^+$ HCCs were relatively rare and constituted only 13% (microarray cohort) to 20% (FACS cohort) of all HCC samples analyzed, we focused on the characterization of EpCAM and CD90. To clarify the cell identity of $EpCAM^+$ or $CD90^+$ cells in primary HCCs, we performed IHC analysis of 18 needle-biopsy specimens of premalignant dysplastic nodules (DNs), 102 surgically resected HCCs, and corresponding NT liver tissues. When examining the expression of EpCAM and CD90 in cirrhotic liver tissue by double-color IHC analysis, we found that $EpCAM^+$ cells and $CD90^+$ cells were distinctively located and not colocalized (Supporting Fig. 1A). Immunoreactivity (IR) to anti-CD90 antibodies (Abs) was detected in vascular endothelial cells (VECs), inflammatory cells, fibroblasts, and neurons, but not in hepatocytes or cholangiocytes, in the cirrhotic liver (Supporting Fig. 1B, panels a,b). IR to anti-EpCAM Abs was detected in hepatic progenitors adjacent to the periportal area and bile duct epithelial cells in liver cirrhosis (Supporting Fig. 1B, panels c,d).

IR to anti-EpCAM Abs was detected in 37 of 102 surgically resected HCCs (Fig. 2A, panel b), but not in 18 DNs (Fig. 2A, panel a). By contrast, no tumor epithelial cells (TECs) showing IR to anti-CD90 Abs were found in any of the 18 DNs or 102 HCCs examined (Fig. 2A, panels c,d). However, we identified $CD90^+$ cells that were morphologically similar to VECs or fibroblasts within the tumor nodule in 37 of the 102 surgically resected HCC tissues (≥5% positive staining in a given area). IR to anti-CD90 Abs was also detected in hepatic mesenchymal tumors (Supporting Fig. 1C, panels a-c), indicating that CD90 is also a marker of liver stromal tumors.

Double-color IHC and immunofluorescence (IF) analysis confirmed the distinct expression of EpCAM and CD90 in HCC (Fig. 2B), consistent with the FACS data (Fig. 1A). Quantitative real-time polymerase chain reaction (qPCR) analysis of sorted $EpCAM^+$, $CD90^+$, and $EpCAM^-$ $CD90^-$ cells after $CD45^+$ cell depletion indicated that the hepatic stem/progenitor markers, *AFP* and *KRT19*, were up-regulated in $EpCAM^+$ cells (red bar), whereas the mesenchymal markers, *KIT* and *FLT1*, were up-regulated in $CD90^+$ cells (orange bar), compared with $EpCAM^-$ $CD90^-$ cells (blue bar) (Fig. 2C). The hepatocyte marker, *CYP3A4*, was down-regulated in $EpCAM^+$ cells and not detected in $CD90^+$ cells, compared with $EpCAM^-$ $CD90^-$ cells. *POU5F1* and *BMI1* were equally up-regulated in both $EpCAM^+$ and $CD90^+$ cells, compared with $EpCAM^-$ $CD90^-$ cells.

EpCAM and CD90 were independently and distinctively expressed in different cellular lineages, so we evaluated the staining of EpCAM and CD90 separately and analyzed the clinicopathological characteristics of surgically resected HCC cases. HCCs were regarded marker positive if ≥5% positive staining was detected in a given area. The existence of $EpCAM^+$

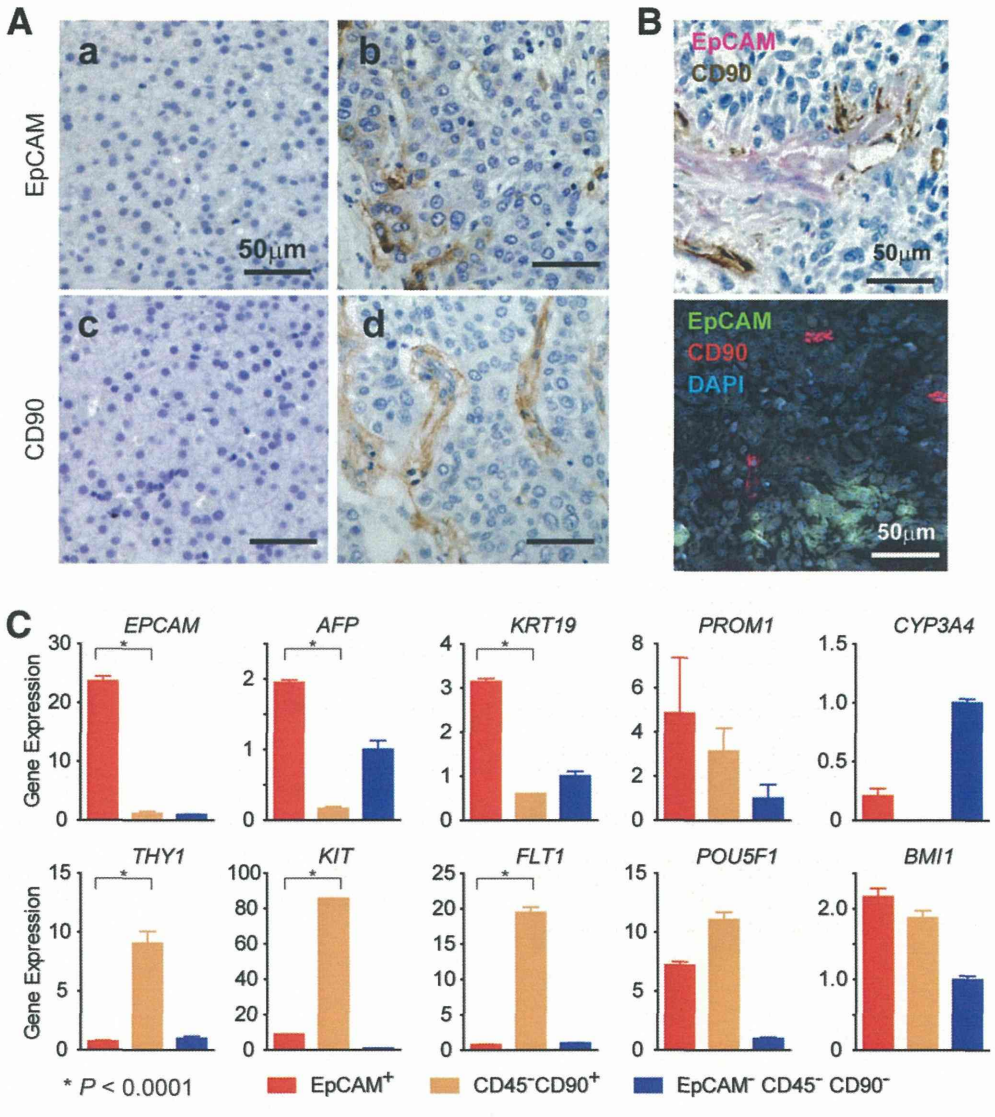

Fig. 2. Distinct EpCAM$^+$ and CD90$^+$ cell populations in HCC. (A) Representative images of EpCAM and CD90 staining in dysplastic nodule (panels a,c) and HCC (panels b,d) by IHC analysis (scale bar, 50 μm). EpCAM (panels a,b) and CD90 (panels c,d) immunostaining is depicted. (B) Upper panel: representative images of EpCAM (red) and CD90 (brown) double staining in HCC by IHC (scale bar, 50 μm). Lower panel: representative images of EpCAM (green) and CD90 (red) staining with 4'6-diamidino-phenylindole (DAPI) (blue) in HCC by IF (scale bar, 50 μm). (C) qPCR analysis of sorted EpCAM$^+$ (red bar), CD90$^+$ (orange bar), or EpCAM$^-$ CD90$^-$ (blue bar) derived from a representative primary HCC. Experiments were performed in triplicate, and data are shown as mean ± standard error of the mean.

cells (≥5%) was characterized by poorly differentiated morphology and high serum AFP values with a tendency for portal vein invasion, whereas the existence of CD90$^+$ cells (≥5%) was associated with poorly differentiated morphology and a tendency for large tumor size (Supporting Tables 2 and 3). Notably, the existence of CD90$^+$ cells was associated with a high incidence of distant organ metastasis, including lung, bone, and adrenal gland, within 2 years after surgery, whereas EpCAM$^+$ cell abundance appeared unrelated to distant organ metastasis.

We evaluated the characteristics of EpCAM$^+$ or CD90$^+$ cells in seven representative HCC cell lines. Morphologically, all EpCAM$^+$ cell lines (HuH1, HuH7, and Hep3B) showed a polygonal, epithelial cell shape, whereas three of four CD90$^+$ cell lines (HLE, HLF, and SK-Hep-1) showed a spindle cell shape (Fig. 3A). EpCAM$^+$ cells were detected in 11.5%, 57.7%, and 99.6% of sorted HuH1, HuH7, and Hep3B cells, respectively. A small CD90$^+$ cell population (0.66%) was observed in PLC/PRL/5, whereas 91.3%, 10.8%, and 59.0% of CD90$^+$ cells were detected in HLE, HLF, and SK-Hep-1, respectively. Compared with primary HCCs, only EpCAM$^+$ or CD90$^+$ cells were detected in liver cancer cell lines under normal culture conditions (Fig. 3B), suggesting that these cell lines contain a relatively pure cell population most likely obtained by clonal selection through the establishment process.

A class-comparison analysis with univariate t tests and a global permutation test (×10,000) of microarray data yielded two main gene clusters up-regulated in EpCAM$^+$ cell lines (HuH1, HuH7, and Hep3B) (cluster I, 524 genes) or in CD90$^+$ cell lines (HLE, HLF, and SK-Hep-1) (cluster II, 366 genes) (Fig. 3C). PLC/PRL/5 showed intermediate gene-expression patterns between EpCAM$^+$ and CD90$^+$ cell lines using this gene set. Pathway analysis indicated that the genes

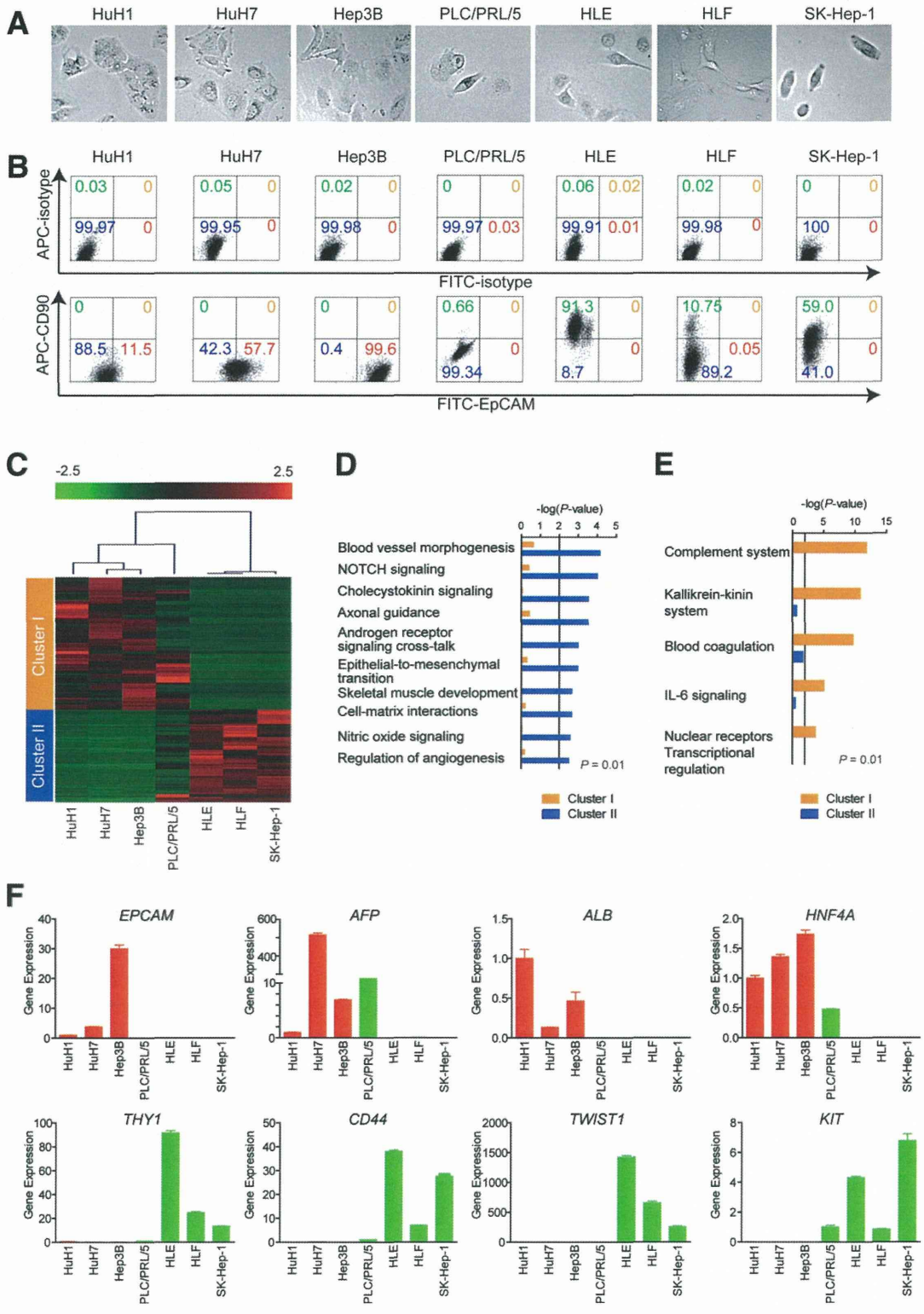

Fig. 3. Characteristics of HCC cell lines defined by EpCAM and CD90. (A) Representative photomicrographs of $EpCAM^{+}CD90^{-}$ and $EpCAM^{-}CD90^{+}$ HCC cell lines. (B) Representative FACS data of $EpCAM^{+}CD90^{-}$ and $EpCAM^{-}$ $CD90^{+}$ HCC cell lines stained with fluorescein isothiocyanate (FITC)-EpCAM and APC-CD90 Abs. (C) Heat-map images of seven HCC cell lines based on 890 EpCAM/CD90-coregulated genes. Each cell in the matrix represents the expression level of a gene in an individual sample. Red and green cells depict high and low expression levels, respectively, as indicated by the scale bar. (D and E) Pathway analysis of EpCAM/CD90-coregulated genes. Canonical signaling pathways activated in cluster I (orange bar) or II (blue bar) with statistical significance ($P < 0.01$) are shown. (F) qPCR of representative differentially expressed genes identified by microarray analysis (C) in seven HCC cell lines.

enriched in cluster II were mainly associated with blood-vessel morpho- and angiogenesis (Fig. 3D). By contrast, the enriched genes in cluster I were significantly associated with known hepatocyte functions ($P < 0.01$) (Fig. 3E). In addition, we identified that the enriched genes in cluster II were significantly associated with neurogenesis, skeletal muscle development, and EMT.

We used qPCR to validate that known hepatic stem cell (HSC) and hepatocyte markers, such as *AFP, EPCAM, ALB*, and *HNF4A* genes, were up-regulated in $EpCAM^+$ cell lines, but not detected in $CD90^+$ cell lines (Fig. 3F). By contrast, genes associated with mesenchymal lineages and EMT, such as *KIT, TWIST1, CD44*, and *THY1*, were strongly up-regulated in $CD90^+$ cell lines.

Unique Tumorigenicity and Metastasis Capacity of Distinct CSCs Defined by EpCAM and CD90. We investigated the tumorigenic capacity of $EpCAM^+$ or $CD90^+$ cells by subcutaneously (SC) injecting 1×10^5 sorted cells of four HCC cell lines (HuH1, HuH7, HLE, and HLF) into nonobese diabetic, severe combined immunodeficient (NOD/SCID) mice. We excluded Hep3B cells for the evaluation of tumorigenicity because almost 100% of cells were EpCAM positive. We further excluded SK-Hep-1 cells from the analysis because they potentially originated from endothelial cells.[12] The highly tumorigenic capacities of $EpCAM^+$ and $CD90^+$ cells were reproduced in HuH1, HuH7, and HLF cell lines, compared with marker-negative cells (Fig. 4A). However, HLE cells did not produce SC tumors, even 12 months after transplantation, in NOD/SCID mice. $EpCAM^+$ cells from HuH1 and HuH7 formed larger tumors more rapidly than $CD90^+$ cells from HLF (Fig. 4B). IHC analyses indicated that $EpCAM^+$ cells did not produce $CD90^+$ cells and *vice versa* in these cell lines *in vivo* (Fig. 4C). $CD90^+$ cells showed a high metastatic capacity, whereas $EpCAM^+$ cells showed no metastasis to the lung when SC tumor volume reached approximately 2,000 (HuH1 and HuH7) or 700 mm^3 (HLF) (Fig. 4D). The high metastatic capacity of PLC/PRL/5 cells, which contain a small population of $CD90^+$ cells, was also confirmed after SC injection into NOD/SCID mice (data not shown). $CD90^+$ cells could divide to generate both $CD90^+$ and $CD90^-$ cells, and $CD90^+$ cells showed a high capacity to invade and form spheroids with overexpression of *TWIST1* and *TWIST2*, which are known to activate EMT programs in HLF cells (Supporting Fig. 2A-D).

We next evaluated the tumorigenic/metastatic capacity of $CD45^-$ tumor cells using 12 fresh primary HCC specimens (P1-P12) that had been surgically resected (Table 2). We further evaluated the tumorigenicity of EpCAM/CD90 sorted cells obtained from xenografts derived from primary HCCs (Supporting Fig. 3A). Of these, we confirmed the tumorigenicity of cancer cells obtained from six primary HCCs after SC injection into NOD/SCID mice within 3 months after transplantation (Fig. 5A; Table 2; Supporting Fig. 3B). $EpCAM^+$ cells derived from four HCCs (P4, P7, P13, and P14) showed highly tumorigenic capacities, compared with $EpCAM^-$ cells. $CD90^+$ cells derived from two HCCs showed equal (P12) or more-tumorigenic capacities (P15), compared with $CD90^-$ cells. Tumorigenicity of $EpCAM^+$ cells was observed in three hepatitis C virus (HCV)-related HCCs and an hepatitis B virus (HBV)-related HCC, whereas tumorigenicity of $CD90^+$ cells was observed in two HBV-related HCCs (Tables 1 and 2).

Using unsorted cells, we compared the frequency of $EpCAM^+$ and $CD90^+$ cells in primary and xenograft tumors and found that $EpCAM^+$ cells remained, but $CD90^+$ cells disappeared, in secondary tumors derived from P4 or P7, whereas $EpCAM^+$ cells disappeared, but $CD90^+$ cells remained, in secondary tumors derived from P12 (Fig. 5B). Morphologically, tumorigenic $EpCAM^+$ cells showed an epithelial cell shape, whereas $CD90^+$ cells showed a mesenchymal VEC shape (Fig. 5C and Supporting Fig. 3C). FACS analysis indicated that P12 HCC cells showed abundant expression of vascular endothelial growth factor receptor (VEGFR) 1 and a vascular endothelial marker endoglin (CD105) (Fig. 5D). By contrast, P4 and P7 HCC cells did not express these vascular endothelial markers (data not shown). Lung metastasis was detected in NOD/SCID mice transplanted with P12 HCC cells, but not in mice transplanted with P4 and P7 HCC cells (Fig. 5E,F).

Taken together, these results suggest that the tumorigenic and metastatic capability of primary HCC may depend on the presence of distinct $EpCAM^+$ or $CD90^+$ CSCs. $EpCAM^+$ cells were associated with a high tumorigenic capacity with hepatic epithelial stem cell features, whereas $CD90^+$ cells were related to the metastatic propensity with VEC features.

Suppression of Lung Metastasis Mediated by $CD90^+$ CSCs by Imatinib Mesylate. We previously demonstrated that Wnt/β-catenin signaling inhibitors could successfully attenuate the tumorigenic capacity of $EpCAM^+$ CSCs in HCC.[8,10] To explore the potential molecular targets activated in $CD90^+$ CSCs, we investigated the expression of the known VEC markers, CD105, VEGFR1 (encoded by *FLT1*), and

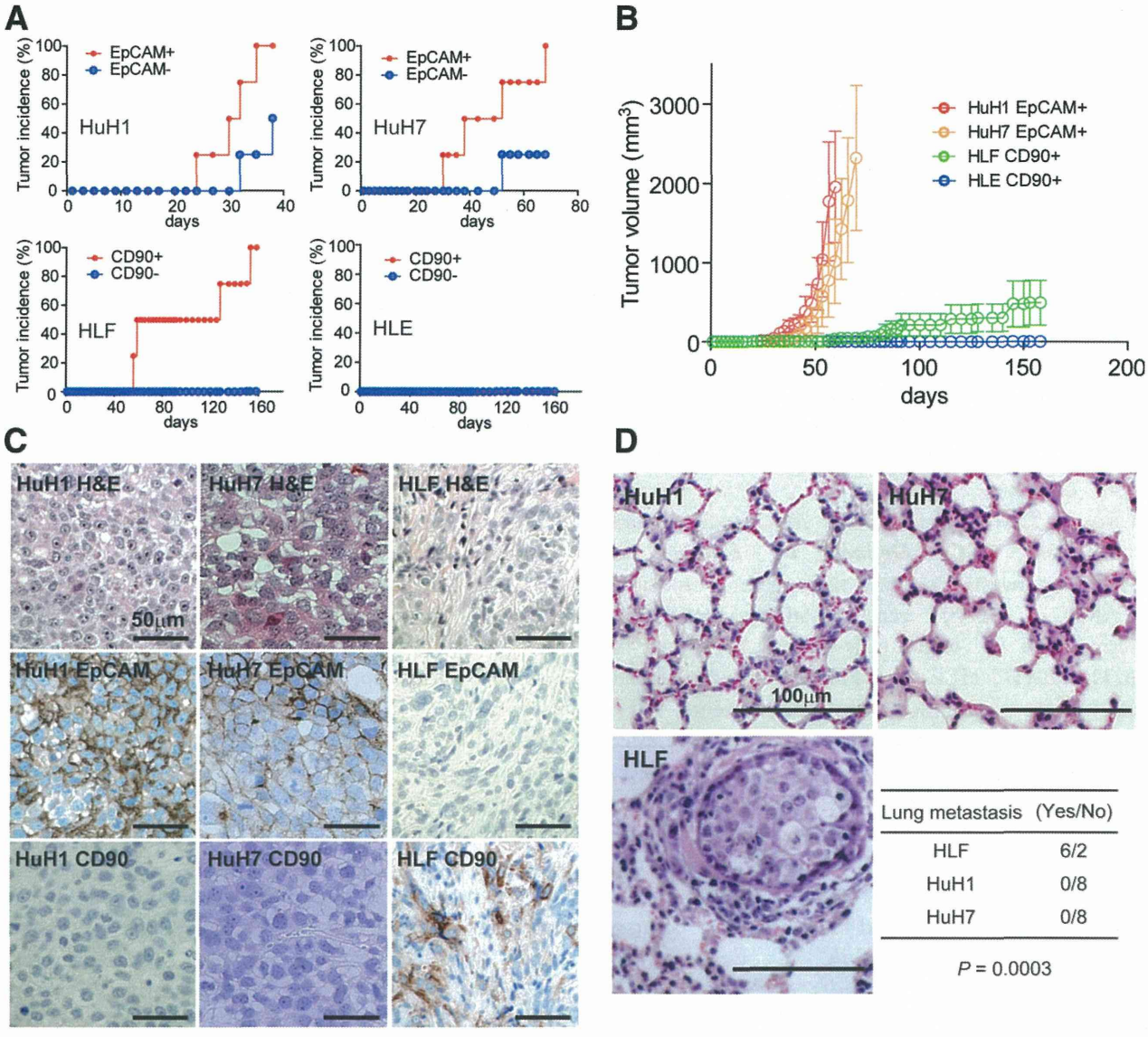

Fig. 4. Distinct tumorigenic/metastatic capacities of HCC cell lines defined by EpCAM and CD90. (A) Tumorigenicity of 1×10^5 cells sorted by anti-EpCAM (HuH1 and HuH7) or anti-CD90 (HLE and HLF) Abs. Data are generated from 8 mice/cell line. (B) Tumorigenic ability of $EpCAM^+$ and $CD90^+$ sorted cells in NOD/SCID mice. Aggressive tumor growth in the SC lesion was observed in $EpCAM^+$ HuH1 or HuH7 cells, compared with $CD90^+$ HLE or HLF cells. $EpCAM^+$ (1×10^5) or $CD90^+$ cells were injected. Tumor-volume curves are depicted as mean ± standard deviation of 4 mice/group. (C) Histological analysis of $EpCAM^+$ or $CD90^+$ cell-derived xenografts. Hematoxylin and eosin (H&E) staining of a SC tumor (upper panels) and IHC of the tumor with anti-EpCAM (middle panels) or anti-CD90 Abs (bottom panels) are shown (scale bar, 50 μm). (D) Metastasis was evaluated macroscopically and microscopically in the left and right lobes of the lung separately in each mouse (n = 4) (scale bar, 100 μm).

c-Kit (encoded by *KIT*), in cell lines and showed that they were abundantly expressed in $CD90^+$ cell lines, but not $EpCAM^+$ cell lines (Fig. 6A). No expression of VEGFR2 was detected in this set of cell lines, suggesting that molecular reagents specifically targeting VEGFR2 may have no effects on $CD90^+$ CSCs. CD44, a stem cell marker that functionally regulates redox status and is a potential target of $CD90^+$ CSCs, was also abundantly expressed in $CD90^+$ cell lines (Supporting Fig. 4A), consistent with previous data.[5,13] No significant difference was detected in the expression of the hematopoietic marker, CD34, or ABCG2 between $EpCAM^+$ and $CD90^+$ cell lines (Supporting Fig. 4A).

Among these molecular targets, we focused on the characterization of c-Kit because the c-Kit tyrosine kinase inhibitor, imatinib mesylate, is readily available, is widely used for the treatment of gastrointestinal stromal tumor with activation of c-Kit, and may have potential antitumor activity against a subset of HCC.[14] We explored the effect of imatinib mesylate on HCC cell lines and found that treatment with 10

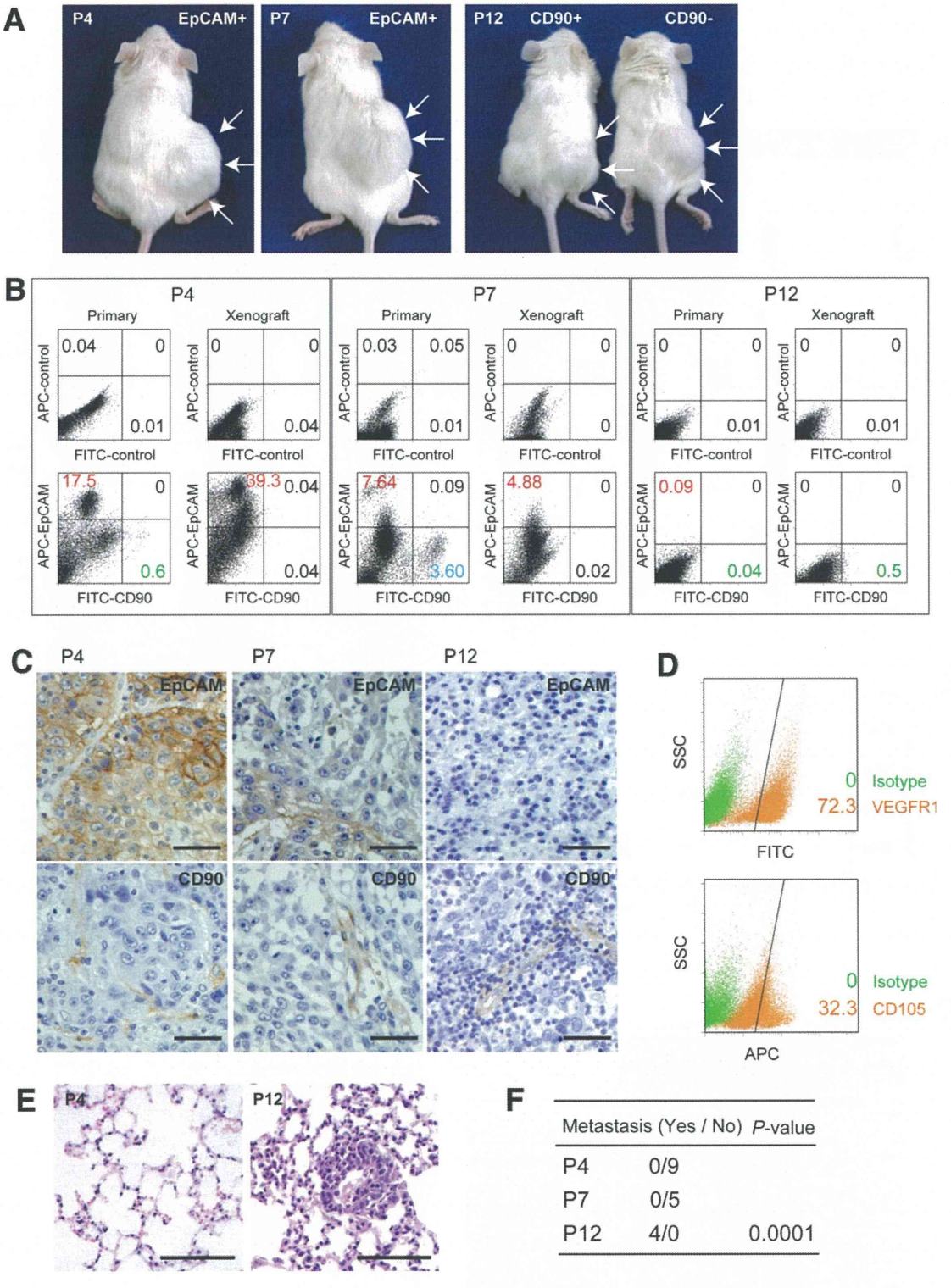

Fig. 5. Tumorigenic/metastatic capacities of EpCAM$^+$ and CD90$^+$ cells in primary HCC. (A) Representative NOD/SCID mice with SC tumors (white arrows) from EpCAM$^+$ P4 or P7 cells (left and middle panels) and CD90$^+$ or CD90$^-$ P12 cells (right panel). (B) FACS analysis of CD90 and EpCAM staining in primary HCCs and the corresponding secondary tumors developed in NOD/SCID mice. Unsorted cells (1×10^6 cells in P4 and P7 or 1×10^5 cells in P12) were SC injected to evaluate the frequency of each marker-positive cell in primary and secondary tumors. (C) IHC analysis of EpCAM and CD90 in primary HCCs P4, P7, and P12 (scale bar, 50 μm). (D) FACS analysis of VEGFR1 (Alexa488) and CD105 (APC) in primary HCC P12. (E) Hematoxylin and eosin staining of lung tissues in P4 and P12 (scale bar, 200 μm). (F) Frequency of lung metastasis in NOD/SCID mice SC transplanted using unsorted primary HCC cells.

μM reduced cell proliferation and spheroid formation in CD90$^+$ cell lines, but had no effect on EpCAM$^+$ cell lines (Supporting Fig. S4B,C).

We further explored the effect of imatinib mesylate *in vivo*. Because EpCAM$^+$ and CD90$^+$ cells reside in the primary HCC, but not in established cell lines, we SC injected HuH7 and HLF cell lines to generate tumors organized by EpCAM$^+$ and CD90$^+$ CSCs. Interestingly, when HLF cells were coinjected with HuH7 cells, EpCAM$^+$ cells could metastasize to the lung, whereas

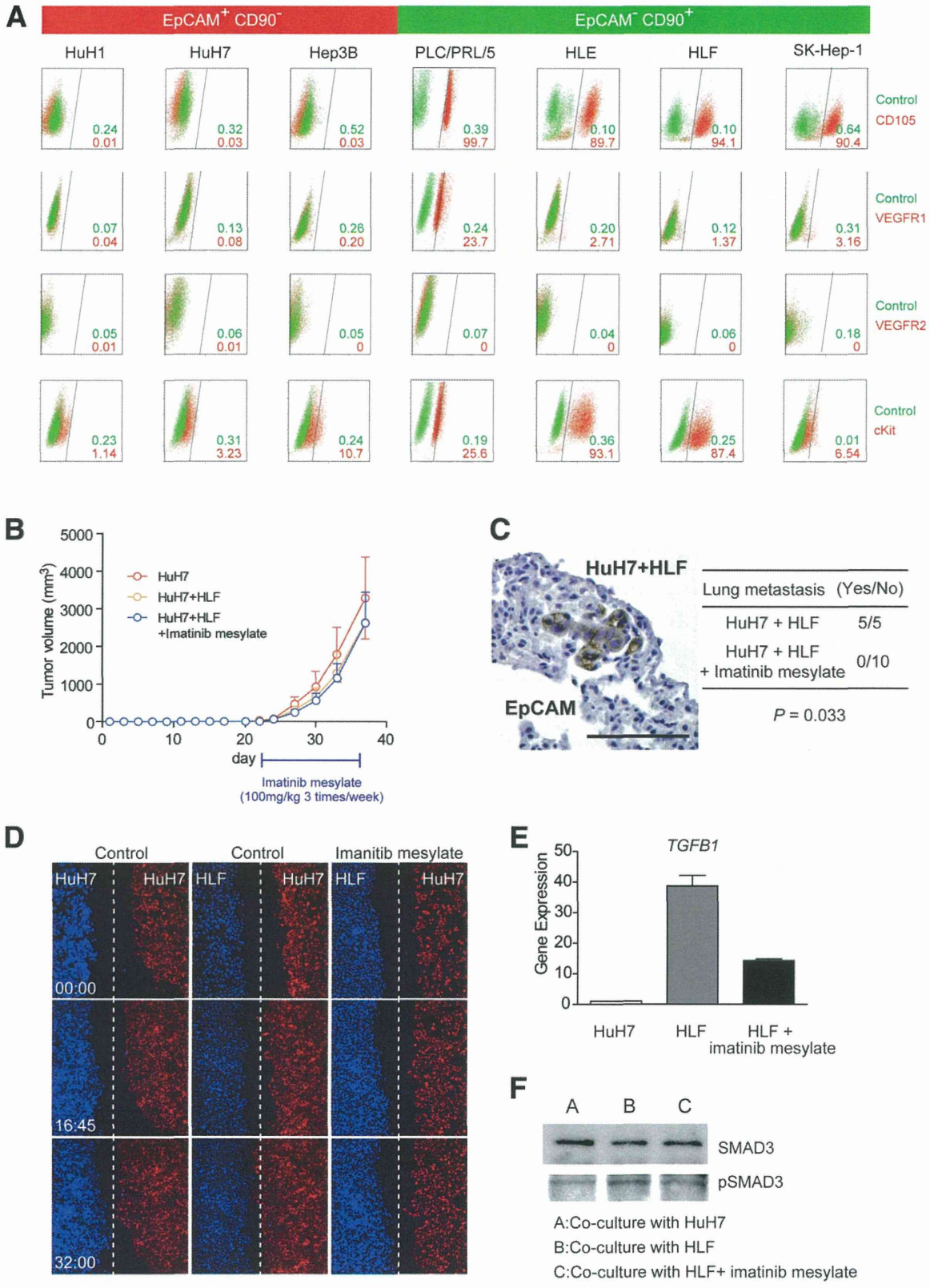

Fig. 6.

SC primary tumors showed no difference in size (Fig. 6B,C). Furthermore, although imatinib mesylate treatment had little effect on the size of primary SC tumors, it significantly suppressed lung metastasis in primary tumors (Fig. 6C). These data suggest that $CD90^+$ cells are not only metastatic to the distant organ, but also help the metastasis of $CD90^-$ cells, including $EpCAM^+$ cells, which originally have no distant metastatic capacity. Our data further suggest that imatinib mesylate can inhibit distant organ metastasis by suppressing $CD90^+$ metastatic CSCs, albeit with little effect on $EpCAM^+$ tumorigenic epithelial stem-like CSCs.

To explore the potential mechanism of how $CD90^+$ cells dictate the metastasis of $EpCAM^+$ cells, we utilized coculture systems and time-lapse image analysis. Wound-healing analysis clearly indicated that motility of HuH7 cells was enhanced when HLF cells were cocultured, and this effect was abolished by imatinib mesylate treatment (Fig. 6D; see Supporting Videos 1-3). HLF cells abundantly expressed *TGFB1*, compared with HuH7 cells, and its expression was dramatically suppressed by imatinib mesylate treatment (Fig. 6E). Mothers against decapentaplegic homolog 3 (Smad3) phosphorylation was augmented in HuH7 cells when cocultured with HLF cells, and this effect was attenuated when cocultured with HLF cells pretreated with imatinib mesylate.

Taken together, our data suggest that liver CSCs are not a single entity. Liver CSCs defined by different markers show unique features of tumorigenicity/metastasis with phenotypes closely associated with committed liver lineages. These distinct CSCs may collaborate to enhance tumorigenicity and metastasis of HCCs.

Discussion

The current investigation demonstrates that CSC marker expression status may be a key determinant of cancer phenotypes, in terms of metastatic propensity and chemosensitivity, to certain molecularly targeted therapies. EpCAM appears to be an epithelial tumorigenic CSC marker, whereas CD90 seems to be a mesenchymal metastatic CSC marker associated with expression of c-Kit and chemosensitivity to imatinib mesylate. Imatinib mesylate may be effective in inhibiting metastasis, but has little effect on primary $EpCAM^+$ HCC cell growth.

We investigated the frequency of three CSC markers (EpCAM, CD90, and CD133) in 15 primary HCCs with a confirmed cell viability of $\geq$70% and found that three HCCs contained $CD133^+$ cells, seven HCCs contained $EpCAM^+$ cells, and all HCCs contained $CD90^+$ cells. Among them, we confirmed the perpetuation of $CD133^+$ cells derived from three HCCs (P7, P12, and P14; data not shown), $EpCAM^+$ cells derived from four HCCs (P4, P7, P13, and P14), and $CD90^+$ cells derived from two HCCs (P12 and P15). Recent studies showed that at least 8 of 21 HCCs (38%)[4] and 13 of 13 HCCs (100%)[5] contained tumorigenic $CD133^+$ or $CD90^+$ CSCs, respectively. Recent IHC and tissue microarray studies also demonstrated that $CD133^+$ and $CD90^+$ cells were detected in 24.8% ($\geq$1% of tumor cells) and 32.2% ($\geq$5% of tumor cells) of HCC cases examined, respectively.[15,16]

One possible explanation of the comparatively low frequency of $CD133^+$ liver CSCs identified in our study is that we used the monoclonal Ab CD133/2, whereas Ma et al. used CD133/1. Another possible explanation is the difference of etiology related to hepatocarcinogenesis. We examined tumorigenicity using 15 HCCs (five HBV related, four HCV related, three non-B, non-C hepatitis [NBNC] related, and three alcohol related) and identified that tumorigenic CSCs were only obtained from HBV- or HCV-related cases. Previous liver CSC studies were performed using HBV-related HCCs,[4,5] and a recent study showed that

Fig. 6. Suppression of lung metastasis mediated by $CD90^+$ CSCs by imatinib mesylate. (A) FACS analysis of seven HCC cell lines stained by APC-CD105, Alexa 488/VEGFR1, APC/VEGFR2, and Alexa 488/c-Kit Abs or isotype control. (B) Tumorigenicity of 5×10^5 HuH7 cells and 2.5×10^5 HuH7 cells plus 2.5×10^5 HLF cells treated with imatinib mesylate or control phosphate-buffered saline (PBS) (200 μL/mouse) orally ingested three times per week (100 mg/kg) for 2 weeks. Data are generated from 5 mice per condition. (C) IHC analysis of EpCAM in lung metastasis detected in NOD/SCID mice SC injected with 2.5×10^5 HuH7 cells and 2.5×10^5 HLF cells. Metastasis was evaluated macro- and microscopically in the left and right lobes of the lung separately in each mouse ($n = 5$) (scale bar, 100 μm). (D) Cell motility of HuH7 cells cocultured with HuH7, HLF, or HLF cells with imatinib mesylate (10 μM) was monitored in a real-time manner by time-lapse image analysis. HuH7 and HLF cells were labeled with the lipophilic fluorescence tracer, DiI (indicated as red) or DiD (indicated as blue), and incubated in a μ-Slide eight-well chamber overnight. Silicone inserts were detached and the culture media replaced with Dulbecco's modified Eagle's medium containing 10% fetal bovine serum, including 0.1% dimethyl sulfoxide (DMSO) (control) or 10 μM of imatinib mesylate dissolved in DMSO (final concentration 0.1%). Immediately after the medium change, cells were cultured at 37°C in 5% CO_2 and time-lapse images were captured for 72 hours. (E) qPCR analysis of *TGFB1* in HuH7 (white bar), HLF (gray bar), and HLF cells pretreated with imatinib mesylate for 24 hours. (F) Smad3 and its phosphorylation evaluated by western blotting. HuH7 cells and HLF cells were harvested in cell culture inserts and treated with DMSO (0.1%) or imatinib mesylate (10 μM) for 24 hours. Cell culture inserts were washed with PBS, cocultured with HuH7 cells for 8 hours, and then removed. HuH7 cells were lysed using radioimmunoprecipitation assay buffer for western blotting. (A) HuH7 cells cocultured with HuH7 cells. (B) HuH7 cells cocultured with HLF cells. (C) HuH7 cells cocultured with HLF cells pretreated with imatinib mesylate.

HBV X may play a role in generating $EpCAM^+$ CSCs.[17] The role of hepatitis virus infection on the generation of CSCs is still unclear and should be clarified in future studies.

We were unable to confirm the tumorigenicity of $CD90^+$ cells in 13 of 15 HCCs, but we observed abundant $CD90^+$ cells in more-advanced HCCs by IHC (data not shown). Tumorigenic $CD90^+$ cells may emerge at a later stage of hepatocarcinogenesis, and the majority of $CD90^+$ cells in early HCCs may be cancer-associated VECs without tumorigenic capacity. Furthermore, we identified tumorigenic $CD90^+$ cells only from HBV-related HCCs, and a recent study suggested that expression of CD90 was associated with HBV infection.[16] We could not detect the small population of $CD90^+$ HuH7 and Hep3B cells reported on by Yang et al. However, because we identified a small population of $CD90^+$ HuH7 cells after treatment with 5-FU (manuscript in preparation), it is conceivable that different cellular stress statuses may explain the observed differences between our findings and those of Yang et al.

The majority of CSC markers discovered thus far are almost identical to those found in healthy tissue stem cells or embryonic stem cells. However, with regard to the liver, the characteristics of healthy hepatic stem/progenitor cells isolated using different stem cell markers are currently under investigation. A recent article examined the characteristics of $EpCAM^+$ and $CD90^+$ oval cells isolated from 2-acetylaminofluorene/partial hepatectomy or D-galactosamine-treated rats.[18] Interestingly, $EpCAM^+$ and $CD90^+$ oval cells represent two distinct populations: The former expresses classical oval cell markers, such as AFP, OV-1, and cytokeratin-19 (CK-19), whereas the latter expresses desmin and alpha smooth muscle actin, but not AFP, OV-1, or CK-19, which indicates that $CD90^+$ populations are more likely to be mesenchymal cells. Another study has demonstrated that mesenchymal cells can interact with HSCs to regulate cell-fate decision.[19] We found that $EpCAM^+$ and $CD90^+$ cells isolated from liver cancer are distinct in terms of gene- and protein-expression patterns in both primary liver cancers and cell lines. Furthermore, these distinct CSCs can interact to regulate the tumorigenicity and metastasis of HCC. Molecular characteristics of $EpCAM^+/CD90^+$ CSCs may potentially reflect the cellular context of healthy stem or progenitor cells.

Although our study strongly indicates that abundant $CD90^+$ cells in a tumor is a risk for distant metastasis in liver cancer, the cell identity and role of $CD90^+$ cells remains elusive. As our IHC, FACS, and xeno-transplantation assays revealed, some $CD90^+$ cells in liver cancer may be cancer-associated VECs or fibroblasts that cannot perpetuate in the xenograft. Recent findings have suggested the importance of stromal cells in tumorigenesis and cancer metastasis,[20-22] so it is possible that these cells may help TECs invade and intravasate into blood vessels, thus playing crucial roles in metastasis.

Another possibility is that $CD90^+$ cells are cancer cells with features of fibroblasts (having undergone EMT) or VECs (having undergone vasculogenic mimicry; VM) that can invade, intravasate, and metastasize cells to distant organs. Recently, two groups reported that a subset of tumor VECs originate from glioblastoma CSCs.[23,24] We successfully confirmed the tumorigenicity and metastatic capacity of $CD90^+$ cells that were morphologically identical to VECs from primary HCCs that could perpetuate in the xenograft. However, a recent study demonstrated that $CD90^+$ HCC cells express glypican-3, a marker detected in hepatic epithelial cells.[25] Further studies are warranted to clarify the nature and role of $CD90^+$ HCC cells.

In our study, $CD90^+$ cells expressed the endothelial marker, c-Kit, CD105, and VEGFR1, and a mesenchymal VEC morphology and high metastatic capacity were confirmed in both primary liver cancer and cell lines. We further confirmed that $CD90^+$ liver cancer cells showed chemosensitivity to imatinib mesylate, suggesting that cancer cells committed to mesenchymal endothelial lineages could be eradicated by the compound. Although imatinib mesylate treatment had little effect on the size of primary tumors originated from both $EpCAM^+$ and $CD90^+$ CSCs, it significantly suppressed lung metastasis *in vivo*. These data are consistent with a recent phase II study demonstrating the tolerable toxicity, but limited efficacy, of imatinib mesylate alone for unresectable HCC patients. Eligibility of imatinib mesylate for advanced HCC patients may be restricted to the HCC subtypes organized by $CD90^+$ CSCs with a highly metastatic capacity and VEC features. Therefore, a combination of compounds targeting $EpCAM^+$ tumorigenic CSCs as well as $CD90^+$ metastatic CSCs may be required for the eradication of HCC and should be tested in the future.

Acknowledgments: The authors thank Ms. Nami Nishiyama and Ms. Mikiko Nakamura for their excellent technical assistance.

References

1. Tsai WL, Chung RT. Viral hepatocarcinogenesis. Oncogene 2010;29: 2309-2324.

2. Chiba T, Kita K, Zheng YW, Yokosuka O, Saisho H, Iwama A, et al. Side population purified from hepatocellular carcinoma cells harbors cancer stem cell-like properties. HEPATOLOGY 2006;44:240-251.
3. Haraguchi N, Ishii H, Mimori K, Tanaka F, Ohkuma M, Kim HM, et al. CD13 is a therapeutic target in human liver cancer stem cells. J Clin Invest 2010;120:3326-3339.
4. Ma S, Tang KH, Chan YP, Lee TK, Kwan PS, Castilho A, et al. miR-130b promotes CD133(+) liver tumor-initiating cell growth and self-renewal via tumor protein 53-induced nuclear protein 1. Cell Stem Cell 2010;7:694-707.
5. Yang ZF, Ho DW, Ng MN, Lau CK, Yu WC, Ngai P, et al. Significance of CD90+ cancer stem cells in human liver cancer. Cancer Cell 2008;13:153-166.
6. Zen Y, Fujii T, Yoshikawa S, Takamura H, Tani T, Ohta T, Nakanuma Y. Histological and culture studies with respect to ABCG2 expression support the existence of a cancer cell hierarchy in human hepatocellular carcinoma. Am J Pathol 2007;170:1750-1762.
7. Lee TK, Castilho A, Cheung VC, Tang KH, Ma S, Ng IO. CD24(+) liver tumor-initiating cells drive self-renewal and tumor initiation through STAT3-mediated NANOG regulation. Cell Stem Cell 2011;9: 50-63.
8. Yamashita T, Budhu A, Forgues M, Wang XW. Activation of hepatic stem cell marker EpCAM by Wnt-beta-catenin signaling in hepatocellular carcinoma. Cancer Res 2007;67:10831-10839.
9. Yamashita T, Forgues M, Wang W, Kim JW, Ye Q, Jia H, et al. EpCAM and alpha-fetoprotein expression defines novel prognostic subtypes of hepatocellular carcinoma. Cancer Res 2008;68:1451-1461.
10. Yamashita T, Ji J, Budhu A, Forgues M, Yang W, Wang HY, et al. EpCAM-positive hepatocellular carcinoma cells are tumor-initiating cells with stem/progenitor cell features. Gastroenterology 2009;136: 1012-1024.
11. Ma S, Chan KW, Hu L, Lee TK, Wo JY, Ng IO, et al. Identification and characterization of tumorigenic liver cancer stem/progenitor cells. Gastroenterology 2007;132:2542-2556.
12. Heffelfinger SC, Hawkins HH, Barrish J, Taylor L, Darlington GJ. SK HEP-1: a human cell line of endothelial origin. In Vitro Cell Dev Biol 1992;28A:136-142.
13. Ishimoto T, Nagano O, Yae T, Tamada M, Motohara T, Oshima H, et al. CD44 variant regulates redox status in cancer cells by stabilizing the xCT subunit of system xc(-) and thereby promotes tumor growth. Cancer Cell 2011;19:387-400.
14. Ramadori G, Fuzesi L, Grabbe E, Pieler T, Armbrust T. Successful treatment of hepatocellular carcinoma with the tyrosine kinase inhibitor imatinib in a patient with liver cirrhosis. Anticancer Drugs 2004;15: 405-409.
15. Kim H, Choi GH, Na DC, Ahn EY, Kim GI, Lee JE, et al. Human hepatocellular carcinomas with "Stemness"-related marker expression: keratin 19 expression and a poor prognosis. HEPATOLOGY 2011;54: 1707-1717.
16. Lu JW, Chang JG, Yeh KT, Chen RM, Tsai JJ, Hu RM. Overexpression of Thy1/CD90 in human hepatocellular carcinoma is associated with HBV infection and poor prognosis. Acta Histochem 2011;113: 833-838.
17. Arzumanyan A, Friedman T, Ng IO, Clayton MM, Lian Z, Feitelson MA. Does the hepatitis B antigen HBx promote the appearance of liver cancer stem cells? Cancer Res 2011;71:3701-3708.
18. Yovchev MI, Grozdanov PN, Zhou H, Racherla H, Guha C, Dabeva MD. Identification of adult hepatic progenitor cells capable of repopulating injured rat liver. HEPATOLOGY 2008;47:636-647.
19. Wang Y, Yao HL, Cui CB, Wauthier E, Barbier C, Costello MJ, et al. Paracrine signals from mesenchymal cell populations govern the expansion and differentiation of human hepatic stem cells to adult liver fates. HEPATOLOGY 2010;52:1443-1454.
20. Dome B, Timar J, Ladanyi A, Paku S, Renyi-Vamos F, Klepetko W, et al. Circulating endothelial cells, bone marrow-derived endothelial progenitor cells and proangiogenic hematopoietic cells in cancer: from biology to therapy. Crit Rev Oncol Hematol 2009;69:108-124.
21. Karnoub AE, Dash AB, Vo AP, Sullivan A, Brooks MW, Bell GW, et al. Mesenchymal stem cells within tumour stroma promote breast cancer metastasis. Nature 2007;449:557-563.
22. Mishra PJ, Humeniuk R, Medina DJ, Alexe G, Mesirov JP, Ganesan S, et al. Carcinoma-associated fibroblast-like differentiation of human mesenchymal stem cells. Cancer Res 2008;68:4331-4339.
23. Ricci-Vitiani L, Pallini R, Biffoni M, Todaro M, Invernici G, Cenci T, et al. Tumour vascularization via endothelial differentiation of glioblastoma stem-like cells. Nature 2010;468:824-828.
24. Wang R, Chadalavada K, Wilshire J, Kowalik U, Hovinga KE, Geber A, et al. Glioblastoma stem-like cells give rise to tumour endothelium. Nature 2010;468:829-833.
25. Ho DW, Yang ZF, Yi K, Lam CT, Ng MN, Yu WC, et al. Gene expression profiling of liver cancer stem cells by RNA-sequencing. PLoS One 2012;7:e37159.

Cancer Immunol Immunother (2013) 62:1421–1430
DOI 10.1007/s00262-013-1447-1

ORIGINAL ARTICLE

Increase in $CD14^+HLA\text{-}DR^{-/low}$ myeloid-derived suppressor cells in hepatocellular carcinoma patients and its impact on prognosis

Fumitaka Arihara · Eishiro Mizukoshi · Masaaki Kitahara · Yoshiko Takata · Kuniaki Arai · Tatsuya Yamashita · Yasunari Nakamoto · Shuichi Kaneko

Received: 15 February 2013 / Accepted: 29 May 2013 / Published online: 14 June 2013

Abstract Myeloid-derived suppressor cells (MDSCs) are known as key immune regulators in various human malignancies, and it is reported that $CD14^+HLA\text{-}DR^{-/low}$ MDSCs are increased in hepatocellular carcinoma (HCC) patients. However, the host factors that regulate the frequency and the effect on the prognosis of HCC patients are still unclear. We investigated these issues and clarified the relationships between a feature of MDSCs and host factors in HCC patients. We examined the frequency of MDSCs in 123 HCC patients, 30 chronic liver disease patients without HCC, and 13 healthy controls by flow cytometric analysis. The relationships between the clinical features and the frequency of MDSCs were analyzed. In 33 patients who received curative radiofrequency ablation (RFA) therapy, we examined the impact of MDSCs on HCC recurrence. The frequency of MDSCs in HCC patients was significantly increased. It was correlated with tumor progression, but not with the degree of liver fibrosis and inflammation. In terms of serum cytokines, the concentrations of IL-10, IL-13, and vascular endothelial growth factor were significantly correlated with the frequency of MDSCs. In HCC patients who received curative RFA therapy, the frequency of MDSCs after treatment showed various changes and was inversely correlated with recurrence-free survival time. The frequency of MDSCs is correlated with tumor progression, and this frequency after RFA is inversely correlated with the prognosis of HCC patients. Patients with a high frequency of MDSCs after RFA should be closely followed and the inhibition of MDSCs may improve the prognosis of patients.

Keywords Myeloid-derived suppressor cells · Hepatocellular carcinoma · Radiofrequency ablation · Recurrence · Cancer

Abbreviations

MDSCs	Myeloid-derived suppressor cells
HCC	Hepatocellular carcinoma
CLD	Chronic liver disease
RFA	Radiofrequency ablation
TACE	Transcatheter arterial chemoembolization
PBMC	Peripheral blood mononuclear cell
Tregs	Regulatory T cells
HLA	Human leukocyte antigen
FGF	Fibroblast growth factor
CCL	Chemokine C–C motif ligand
G-CSF	Granulocyte colony stimulating factor
GM-CSF	Granulocyte macrophage colony stimulating factor
IP	Interferon gamma-induced protein
MCP	Monocyte chemoattractant protein
MIP	Macrophage inflammatory protein
PDGF	Platelet-derived growth factor
RANTES	Regulated upon activation, normal T cell expressed and secreted
TNF	Tumor necrosis factor
VEGF	Vascular endothelial growth factor

Electronic supplementary material The online version of this article (doi:10.1007/s00262-013-1447-1) contains supplementary material, which is available to authorized users.

F. Arihara (✉) · E. Mizukoshi · M. Kitahara · Y. Takata · K. Arai · T. Yamashita · S. Kaneko
Department of Gastroenterology, Graduate School of Medicine, Kanazawa University, 13-1, Takara-machi, Kanazawa, Ishikawa 920-8641, Japan
e-mail: bnkyo78@gmail.com; arihara@m-kanazawa.jp

Y. Nakamoto
Second Department of Internal Medicine, Faculty of Medical Sciences, University of Fukui, Matsuoka, Fukui, Japan

JAK Janus kinase
STAT Signal transducer and activator of transcription

Introduction

Hepatocellular carcinoma (HCC) is one of the most common malignancies and the third leading cause of cancer mortality globally [1, 2]. Current treatment options including surgical resection, radiofrequency ablation (RFA), liver transplantation, chemotherapy, transcatheter arterial chemoembolization (TACE), and sorafenib are reported to improve survival in HCC patients [3–7]. However, despite curative treatments for HCC, tumor recurrence rates remain high and the survival of those who have advanced HCC remains unsatisfactory [3–7]. Therefore, the development of new anti-tumor treatments for HCC remains an urgent and important field of research.

To overcome the limitations of these treatments, several immunotherapies have been developed as attractive strategies for HCC. In several studies of HCC immunotherapy, effective induction of immune-mediated cells by tumor antigen-derived peptides or antigen-presenting cells showed anti-tumor effects, but the population of patients who exhibited such effects was very small [8–12].

In previous studies, it was reported that many kinds of tumor generate a number of immune-suppressive mechanisms [13–15]. Recently, myeloid-derived suppressor cells (MDSCs) have been characterized as key immune regulators in various human cancers [15–24]. They show the capacity to inhibit T cell function and promote tumor development [15, 25]. Human MDSCs are a heterogeneous population that shows $CD11b^+$, $CD33^+$, $HLA\text{-}DR^{-/low}$ and can be divided into granulocytic $CD14^-$ and monocytic $CD14^+$ subtypes [26–28]. In most recent studies, it has been reported that $CD14^+HLA\text{-}DR^{-/low}$ MDSCs were increased in HCC patients and the cells inhibited the function of T cells through the induction of regulatory T cells (Tregs) [24]. Tregs represent 5–10 % of $CD4^+$ T cells and can suppress the activation and proliferation of $CD4^+$ and $CD8^+$ T cells [14, 29]. It was reported that an increased frequency of circulating Tregs was associated with poor survival of HCC patients [30]. Understanding the inhibitory mechanism of MDSCs and controlling their function are very important to develop more effective immunotherapy for HCC.

In this study, we investigate the host factors that are associated with the frequency of MDSCs in HCC patients and the effect of MDSCs on the prognosis of patients and clarify the relationships between a feature of MDSCs and host factors in HCC patients.

Materials and methods

Patients and healthy controls

Blood samples were obtained from a total of 123 HCC patients, 26 chronic liver disease (CLD) patients without HCC, and 13 healthy controls. The diagnosis of HCC was histologically confirmed in 68 patients. For the remaining 55 patients, diagnosis was made by dynamic CT or MRI. Patient characteristics and disease classification are shown in Suppl. table 1. All CLD patients without HCC underwent percutaneous liver biopsy to evaluate the disease severity according to the Metavir scoring system. In 33 patients treated with curative percutaneous RFA, blood samples were obtained on the day of treatment and 2–4 weeks after treatment, and we observed recurrence of these patients with periodic imaging studies. All subjects provided written informed consent to participate in this study in accordance with the Declaration of Helsinki. This study was approved by the regional ethics committee (Medical Ethics Committee of Kanazawa University).

Cell isolation and flow cytometric analysis

Peripheral blood mononuclear cells (PBMCs) were separated as described below; heparinized venous blood was diluted in phosphate-buffered saline (PBS) and loaded on Ficoll-Histopaque (Sigma, St. Louis, Mo.) in 50 ml tubes. After centrifugation at 2,000 rpm for 20 min at room temperature, PBMCs were harvested from the interphase, resuspended in PBS, centrifuged at 1,400 rpm for 10 min, and finally resuspended in complete culture medium consisting of RPMI (GibcoBRL, Grand Island, NY), 10 % heat inactivated FCS (Gibco BRL), 100 U/ml penicillin, and 100 μg/ml streptomycin (Gibco BRL). PBMCs were resuspended in RPMI 1,640 medium containing 80 % FCS and 10 % dimethyl sulfoxide and cryopreserved until use. The viability of cryopreserved PBMCs was 60–70 %. In some patients, fresh and cryopreserved PBMCs were obtained from the same sample. To determine the frequency and phenotype of MDSCs and Tregs, multicolor fluorescence-activated cell sorting analysis was carried out using the Becton–Dickinson FACSAria II system. The following anti-human monoclonal antibodies were used: anti-CD4 (Becton–Dickinson), anti-CD11b (Becton–Dickinson), anti-CD14 (Becton–Dickinson), anti-CD15 (Becton–Dickinson), anti-CD25 (Becton–Dickinson), anti-CD33 (Becton–Dickinson), anti-CD127 (Becton–Dickinson), and anti-HLA-DR (Becton–Dickinson).

Suppression assay

$CD14^+HLA\text{-}DR^{-/low}$ MDSCs and $CD14^+HLA\text{-}DR^+$ cells were sorted using the Becton–Dickinson FACSAria II

system. 2×10^4 PBMCs were cultured and stimulated with 1 μg/ml plate-bound anti-CD3 (eBioscience) and 1 μg/mL soluble anti-CD28 (eBioscience) in 96-well round-bottomed plates. 24 h later, to determine the suppressive ability of MDSCs, increasing concentrations of MDSCs were added to the stimulated PBMCs. Proliferation was measured by ^{3}Hincorporation after 72 h. [^{3}H] thymidine was added, and cell proliferation was measured by incorporation of radiolabeled thymidine for 24 h.

Cytokine and chemokine profiling

Blood samples were collected from patients at the same time of PBMC isolation. After centrifugation at 3,000 rpm for 10 min at 4 °C, serum fractions were obtained and stored at −20 °C until use. Serum levels of various cytokines and chemokines were measured using the Bio-Plex Protein Array System. Briefly, frozen serum samples were thawed at room temperature and diluted 1:4 in sample diluents; 50 μl aliquots of the diluted sample was added in duplicate to the wells of 96-well microtiter plates containing the coated beads for a validated panel of human cytokines and chemokines according to the manufacturer's instructions. The following 27 cytokines and chemokines were targeted: IL-1β, IL-1 receptor antagonist (IL-1Ra), IL-2, IL-4, IL-5, IL-6, IL-7, IL-8, IL-9, IL-10, IL-12(p70), IL-13, IL-15, IL-17, basic fibroblast growth factor (FGF), eotaxin (chemokine C–C motif ligand (CCL) 11), G-CSF, GM-CSF, IFN-γ, interferon gamma-induced protein (IP)-10, monocyte chemoattractant protein (MCP)-1, macrophage inflammatory protein (MIP)-1α, MIP-1β, platelet-derived growth factor (PDGF)-BB, regulated upon activation, normal T cell expressed and secreted (RANTES), TNF-α, and vascular endothelial growth factor (VEGF). Nine standards (ranging from 0.5 to 32,000 pg/ml) were used to generate calibration curves for each cytokine. Data acquisition and analysis were performed using Bio-Plex Manager software version 4.1.1.

Statistical analysis

Data are expressed as the mean ± SD. Chi-squared test with Yates' correction, unpaired t test, Mann–Whitney U test, and Kruskal–Wallis were used for univariate analysis of two groups that were classified according to the frequency of MDSCs. The probability of tumor recurrence-free survival was estimated using the Kaplan–Meier method. The Mantel-Cox log-rank test was used to compare curves between groups. The prognostic factors for tumor recurrence-free survival were analyzed for statistical significance by the Kaplan–Meier method (univariate) and the Cox proportional hazard model (multivariate). Variables with $p < 0.1$ were entered into multivariate logistic regression analysis. A level of $p < 0.05$ was considered significant.

Results

$CD14^+HLA\text{-}DR^{-/low}$ MDSCs are increased in the peripheral blood of HCC patients

We analyzed the peripheral blood of 123 patients with HCC, 26 CLD patients without HCC, and 13 healthy donors for the prevalence of $CD14^+HLA\text{-}DR^{-/low}$ MDSCs. Because the PBMCs are tested after Ficoll, some cells may be lost. Therefore, we examined the population of MDSCs as a percentage of total $CD14^+$ cells by flow cytometry after cell surface labeling for the expression of HLA-DR (Fig. 1a). $CD14^+HLA\text{-}DR^{-/low}$ population in PBMCs of HCC patients represented 3.2–56.8 % of the $CD14^+$ cells. The frequency of $CD14^+HLA\text{-}DR^{-/low}$ MDSCs/$CD14^+$ cells in cryopreserved PBMCs correlated with that in fresh PBMCs (Fig. 1b). Therefore, we analyzed the frequency of $CD14^+HLA\text{-}DR^{-/low}$ MDSCs/$CD14^+$ cells using cryopreserved PBMCs.

To confirm the function of these cells, sorted $CD14^+HLA\text{-}DR^{-/low}$ MDSCs and $CD14^+HLA\text{-}DR^+$ (control) cells were added at different ratios to autologous anti-CD3/CD28-stimulated PBMCs, and the proliferation was measured by ^{3}Hincorporation. $CD14^+HLA\text{-}DR^{-/low}$ MDSCs of HCC patients significantly decreased autologous PBMC proliferation (Fig. 1c). On the other hand, $CD14^+HLA\text{-}DR^+$ (control) cells could not suppress the autologous PBMC proliferation.

As shown in Fig. 1d, the frequency of MDSCs was significantly higher in HCC patients (19.0 %) than in healthy donors (9.4 %) ($p < 0.01$). Overall frequencies of $CD14^+$ cells did not differ significantly between the groups (Fig. 1e). Individual frequencies of MDSCs of all the patients and healthy donors are represented as scatter plots (Fig. 2a). The frequency of MDSCs was correlated with the stage of HCC (stage III and IV: 22.3 % ($n = 46$) vs. stage I and II: 17.0 % ($n = 77$), $p < 0.01$) and was significantly higher in HCC patients than CLD patients without HCC and healthy donors. Interestingly, there was no difference between CLD patients without HCC and healthy donors. Moreover, these numbers did not change depending on the degree of fibrosis or inflammatory activity of the liver (Fig. 2b, c).

In previous reports, granulocytic MDSCs were defined in combination with several surface markers including CD14, CD15, CD11b, CD33, CD66b, and HLA-DR in several cancers. Therefore, we examined the frequency of $CD15^+CD14^-CD11b^+CD33^+$ cells in 37 HCC patients and 11 healthy donors (Suppl. figure 1A). Although there was no statistical significant difference, the frequency of

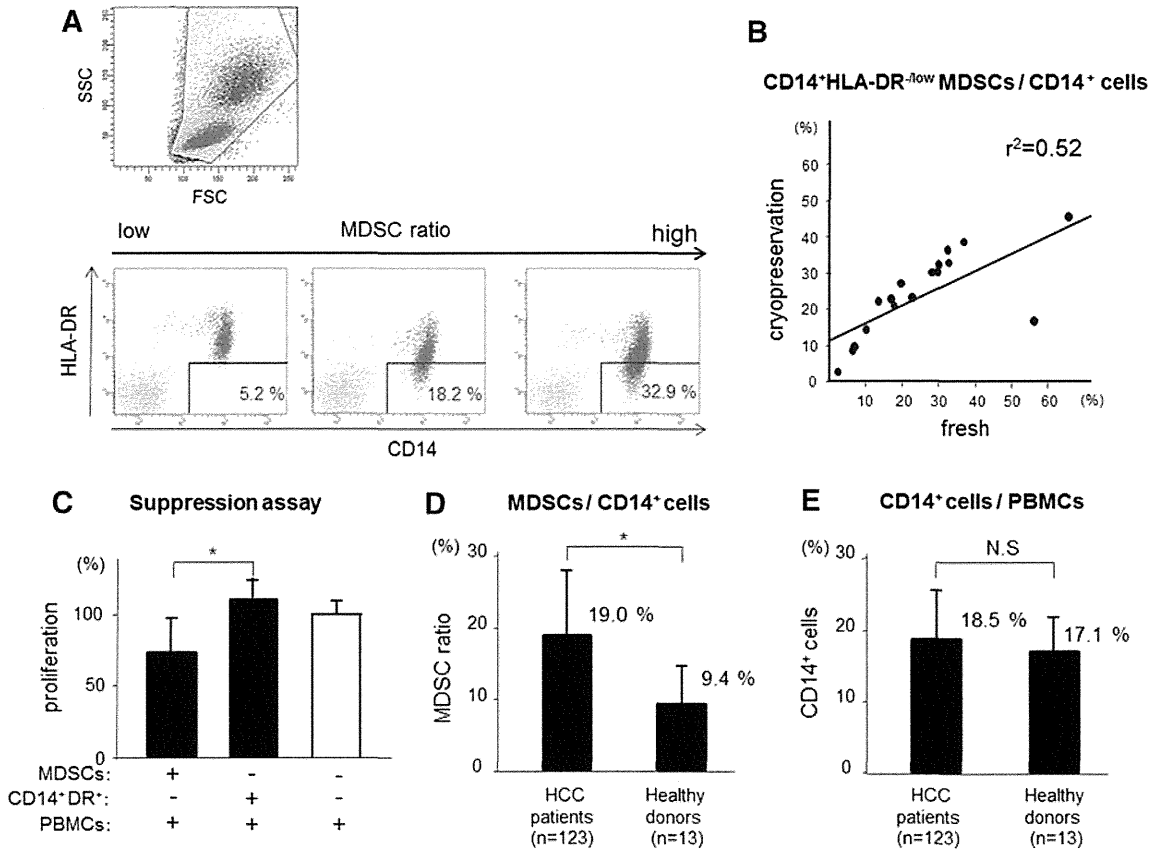

Fig. 1 **a** Flow cytometry shows $CD14^{+}HLA\text{-}DR^{-/low+}$ MDSCs. PBMCs from patients and healthy donors were labeled with anti-CD14 and HLA-DR. Three staining examples of HCC patients are shown in the order from a small number (*left*) to a large number (*right*). **b** The increase in $CD14^{+}HLA\text{-}DR^{-/low}$ MDSCs/$CD14^{+}$ cells in cryopreserved PBMC correlated with that in fresh PBMC ($r^2 = 0.52$). **c** Proliferation of PBMCs stimulated by anti-CD3/28 in the presence or absence of MDSCs was measured by ^{3}Hincorporation assay. $CD14^{+}HLA\text{-}DR^{-/low}$ MDSCs significantly decreased autologous PBMC proliferation ($n = 4$; *, $p < 0.05$). **d** The frequency of MDSCs was significantly higher in HCC patients than healthy donors (*, $p < 0.01$). **e** Overall frequencies of $CD14^{+}$ cells did not differ significantly

$CD15^{+}CD14^{-}CD11b^{+}CD33^{+}$ cells in HCC patients was higher than that in healthy donors (2.84 vs. 2.06 %, $p = 0.073$) (Suppl. figure 1B). The frequency was correlated with the stage of HCC (stage III and IV: 3.69 % ($n = 13$) vs. stage I and II: 2.39 % ($n = 24$), $p = 0.022$) (Suppl. figure 1C).

Relationship between the frequency of Tregs and MDSCs

It is well known that the frequency of circulating Tregs is increased and correlated with disease progression in HCC patients. The frequency of $CD4^{+}$ $CD25^{+}$ $CD127^{-/low}$ Tregs was significantly increased in HCC patients (Suppl. figure 2A) and associated with tumor progression (Suppl. figure 2B). However, there was not a strong correlation between the frequency of MDSCs and Tregs in our study (Suppl. figure 2C).

Identification of host factors related to the frequency of MDSCs in HCC patients

We divided the HCC patients into two groups using the threshold of an MDSC ratio of 22 %. This threshold is the average +2SD of the MDSC ratio in non-HCC patients. In the group with high frequency, the tumor factors including size, multiplicity, and stage were significantly worse (tumor size, 28.3 vs. 24.4 mm; tumor multiplicity (multiple/solitary), 27/12 vs. 42/42; TNM stage (I and II vs. III and IV), 17/22 vs. 60/24, $p < 0.05$) (Table 1). Moreover, hepatic reserve was also worse in the group with high frequency (Child-Pugh classification (A/B/C), 20/17/2 vs. 64/16/4, $p < 0.05$). In addition, overall survival was significantly shortened in the group with high frequency (hazard ratio 2.67, $p = 0.008$) (Suppl. figure 3A), and recurrence-free survival was also significantly shortened (hazard ratio 1.94, $p = 0.010$) (Suppl. figure 3B).

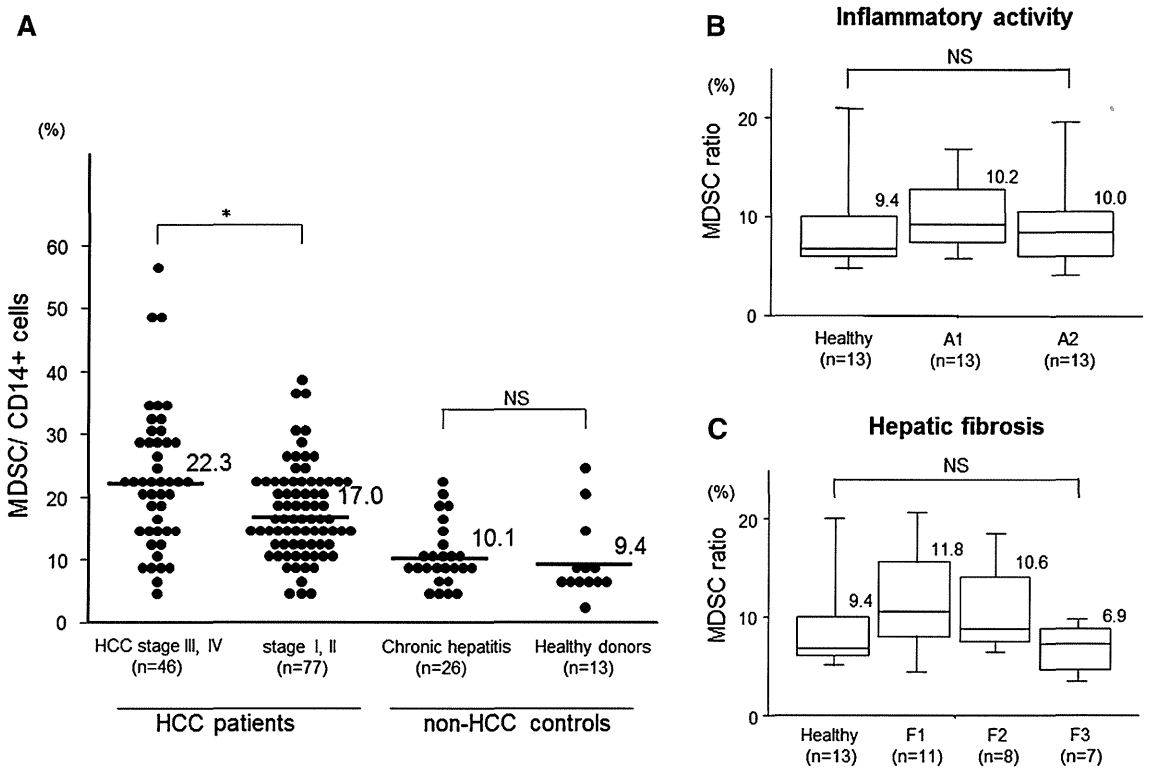

Fig. 2 **a** Scatter plots of MDSC ratio ($CD14^+HLA\text{-}DR^{-/low}$ MDSCs/ $CD14^+$ cells) in patients and healthy donors. The frequency of MDSCs was significantly increased in HCC patients compared with that in non-HCC controls. Moreover, the frequency of MDSCs was correlated with tumor progression (stage III and IV: 22.3 % ($n = 46$) vs. stage I and II: 17.0 % ($n = 77$); *, $p < 0.05$). In non-HCC controls, there was no significant difference in the frequency of MDSCs. **b**, **c** In non-HCC patients, the frequency of MDSCs did not change depending on the degree of fibrosis or inflammatory activity of the liver according to the Metavir scoring system

Relationship between serum cytokine levels and the frequency of MDSCs

In previous studies, the balance of circulating cytokines was thought to promote accumulation and activation of MDSCs [18, 31–34]. Therefore, we examined the relationship between serum cytokine levels and the frequency of MDSCs in HCC patients. In 54 HCC patients, serum levels of cytokines and chemokines were measured using the Bio-Plex Protein Array system. Serum concentrations of IL-10, IL-13, and VEGF were significantly increased in the group with a high frequency of MDSCs (Table 2). In addition, there was a positive correlation between these cytokine levels in serum and the frequency of MDSCs. We also examined the relationship between serum cytokine levels and the frequency of Tregs. We divided the HCC patients into two groups using the threshold of 7 %, which is the average +2SD of the % of Tregs among $CD4^+$ cells in non-HCC patients. Serum concentration of IL-10 was significantly increased in the group with a high frequency of Tregs (Suppl. table 2).

Kinetics of MDSCs before and after curative RFA therapy

We examined the frequency of MDSCs before and after curative RFA therapy in 33 patients. For this analysis, blood samples were obtained on the day of treatment (before) and 2–4 weeks after treatment (after). The frequency of MDSCs was significantly decreased after RFA therapy (18.0 to 15.5 %, $p < 0.05$) (Fig. 3a). However, in several patients, the frequency of MDSCs remained at a high level compared with that in non-HCC patients. The clinical parameters before RFA were not statistically different between the patients with and without a high frequency of MDSCs after RFA (Suppl. table 3).

Next, we followed up these patients for recurrence and analyzed the risk factors. If a high frequency of MDSC was observed after curative RFA therapy, the recurrence-free survival was significantly shortened (Fig. 3b). In contrast, the frequency of MDSCs before treatment did not affect the recurrence. In univariate analysis for recurrence, post-treatment MDSC ratio ≥22 % ($p = 0.023$) and tumor

Table 1 Clinical findings and MDSCs

Clinical characteristics	MDSC ratio ≥22 ($n = 39$)	MDSC ratio <22 ($n = 84$)	p value
Age (year)	68.5	70.1	0.646
Sex (M/F)	29/10	54/30	0.267
AST (IU/l)	62.0	61.5	0.543
ALT (IU/l)	47.1	53.9	0.759
LDH (IU/l)	225	218	0.832
γGTP (IU/l)	78.0	76.0	0.252
Platelet (10^4/μl)	10.9	10.6	0.884
Prothrombin time (%)	75.2	82.3	0.045
Serum albumin (g/dl)	3.53	3.68	0.120
Total bilirubin (mg/dl)	1.21	0.94	0.286
WBC (/μl)	3910	3610	0.235
Neutrophil (%)	63.2	59.4	0.093
Lymphocyte (%)	26.1	29.5	0.047
Total cholesterol (mg/dl)	151	149	0.926
HbA1c (%)	5.27	5.43	0.197
Type IV collagen 7S (ng/ml)	8.2	7.3	0.086
DCP (mAU/ml)	5157	432	0.561
AFP (ng/ml)	1301	934	0.240
Tumor size (mm)	28.3	24.4	0.014
Tumor multiplicity (multiple/solitary)	27/12	42/42	0.046
TNM stage (I plus II/III plus IV)	17/22	60/24	0.003
Child-Pugh (A/B/C)	20/17/2	64/16/4	0.015
Etiology (HCV/HBV/others)	21/11/7	61/11/12	0.081
$CD4^+$ $CD25^+$ $CD127^{-/low}$ Tregs/ $CD4^+$ cells (%)	7.04	6.70	0.281

AST aspirate aminotransferase, *ALT* alanine aminotransferase, *LDH* lactic dehydrogenase, *γGTP* gamma glutamyltransferase, *WBC* white blood cell, *Hb* hemoglobin, *DCP* des-gamma-prothrombin, *AFP* alpha-fetoprotein, *HCV* hepatitis C virus, *HBV* hepatitis B virus, *Tregs* regulatory T cells

Chi-squared test with Yates' correction, unpaired t test, Mann–Whitney U test, and Kruskal–Wallis test were used for univariate analysis of two groups that were classified according to the frequency of MDSCs

multiplicity ($p = 0.010$) were significantly associated with HCC recurrence (Table 3). In multivariable analysis for recurrence, considering the variables in the univariate analysis with $p < 0.1$, only post-treatment MDSC ratio ≥22 % (HR 3.906, $p = 0.014$) was extracted as a significant risk factor for recurrence.

Discussion

MDSCs are expanded in pathological conditions such as malignancy, infection, or trauma and consist of a heterogeneous population of immature myeloid cells [15, 25]. In pathological conditions, immature myeloid cells are blocked to differentiate into mature macrophages, dendritic cells, or granulocytes; as a result, MDSCs are accumulated [15, 25]. MDSCs strongly inhibit anti-tumor immune response through a number of mechanisms [15, 25]. As monocytic subsets of MDSCs, $CD14^+HLA\text{-}DR^{-/low}$ MDSCs have been reported in various malignancies, including melanoma, multiple myeloma, prostate cancer, and bladder cancer [18, 20, 22, 35]. In the most recent study, Hoechst et al. [24] reported that $CD14^+HLA\text{-}DR^{-/low}$ MDSCs were significantly increased in HCC patients and they suppressed T cell functions through the induction of $CD4^+CD25^+Foxp3^+$ Treg.

In the present study, in addition to an increase in the number of MDSCs in HCC patients, we observed that the frequency was correlated with the progression of HCC. Consistent with our results, it has also been reported that the frequency of $CD14^+HLA\text{-}DR^{-/low}$ MDSCs was correlated with tumor progression in patients with other cancers, such as melanoma, prostate cancer, and bladder cancer [22, 35, 36]. However, the mechanisms behind the increase in MDSCs in advanced cancer patients are still unclear. As is well known, there is a close relationship between hepatocarcinogenesis and histological status of underlying liver [37, 38]. Therefore, the advance of hepatic fibrosis and the increase in inflammatory cell infiltration into liver might result in an increase in MDSCs following the progression of HCC. However, there was no relationship between the frequency of $CD14^+HLA\text{-}DR^{-/low}$ MDSCs and underlying liver status in our study. From our observations, increase in MDSCs was only correlated with tumor progression, but not with hepatic fibrosis or disease activity of CLD. This finding suggests that the expansion of $CD14^+HLA\text{-}DR^{-/low}$ MDSCs was mostly derived from the tumor environment itself, but not from inflammation or fibrosis of liver tissue around the tumor. The finding that a significant decrease in the frequency of circulating $CD14^+HLA\text{-}DR^{-/low}$ MDSCs is observed in most patients with curative treatment in this study supports this hypothesis. On the other hand, Tregs were also increased in HCC patients and associated with the progression of HCC. Though it was reported that MDSCs suppressed T cell function through the induction of Tregs, there was not a strong correlation between the frequencies of these two immunosuppressive cells.

Regarding the mechanism of MDSC expansion, we also analyzed the relationship between the serum cytokine levels and the frequency of MDSCs. We observed that the serum concentrations of IL-10, IL-13, and VEGF were significantly increased in the group with high frequency of MDSCs and there was a positive correlation between these cytokine levels and the frequency of MDSCs. Moreover, although there was no significant difference, the serum

Table 2 Serum cytokines and MDSCs

Cytokine	Healthy donor (mean) ($n = 13$)	MDSC ratio ≥ 22 (mean) ($n = 21$)	Range	MDSC ratio < 22 (mean) ($n = 31$)	Range	p value
IL-1ra	34.2	97.0	(21.5–600)	40.3	(3.4–151)	0.057
IL-2	10.5	38.1	(4.3–54.3)	11.3	(0.9–49.7)	0.055
IL-4	2.6	5.75	(1.47–11.9)	5.03	(0.71–10.9)	0.159
IL-6	9.9	21.5	(1.2–130)	10.1	(0.2–97.2)	0.065
IL-8	24.5	64.7	(10.9–291)	35.1	(6.2–142)	0.156
IL-10	2.76	6.01	(0.8–11.5)	2.81	(0.1–12.0)	0.003
IL-12(p70)	14.6	33.3	(0.6–140)	17.6	(1.4–57)	0.058
IL-13	7.6	13.1	(1.2–33.6)	8.2	(2.7–22.9)	0.015
IL-17	15.7	23.5	(4.6–70)	20.8	(2.1–119)	0.115
Eotaxin	104	141	(51.9–493)	124	(26.3–331)	0.675
G-CSF	7.9	13.2	(2.7–41.3)	8.7	(0.5–17.9)	0.050
IFN-γ	52.6	95.4	(23.1–417)	69.9	(2.5–238)	0.136
MCP-1	20.2	26.8	(8.4–114)	23.8	(3.5–77)	0.744
MIP-1b	97.6	120	(58.3–490)	108	(39.7–263)	0.508
PDGF	4012	4375	(1,312–10,136)	4013	(831–13,557)	0.484
RANTES	2978	2890	(1,040–4,826)	3184	(599–6,165)	0.186
TNF-α	10.5	34.9	(0.1–175)	27.6	(2.9–105)	0.756
VEGF	34.6	101.7	(22.5–371)	59.5	(9.3–183)	0.045

IL interleukin, *G-CSF* granulocytic colony stimulating factor, *IFN* interferon, *MCP* monocyte chemoattractant protein, *MIP* macrophage inflammatory protein, *PDGF* platelet-derived growth factor, *RANTES* regulated upon activation, normal T cell expressed and secreted, *TNF* tumor necrosis factor, *VEGF* vascular endothelial growth factor

Mann–Whitney *U* test was used for univariate analysis of two groups that were classified according to the frequency of MDSCs

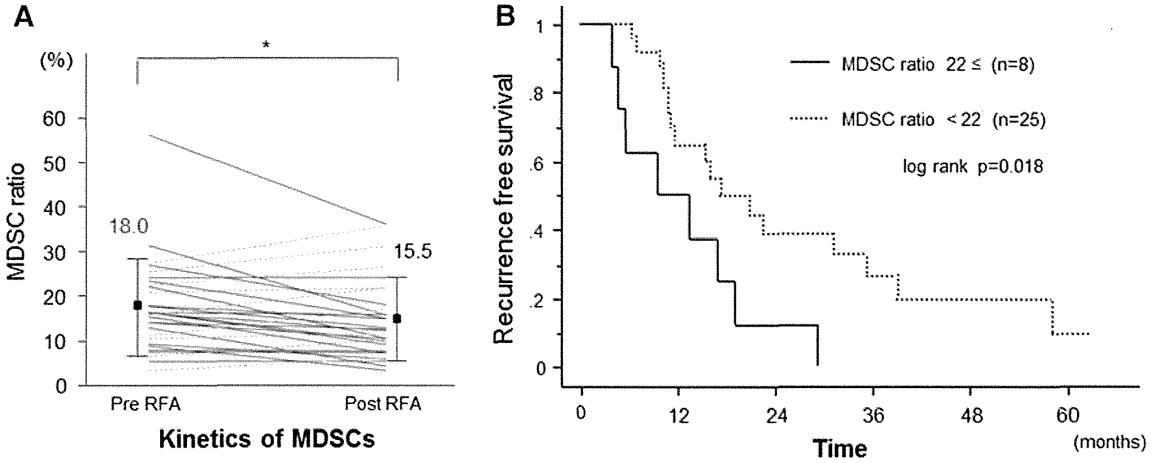

Fig. 3 **a** In 33 HCC patients who received curative RFA therapy, the frequency of MDSCs was significantly decreased after treatment. However, in several patients, the frequencies were increased after treatment (*dotted lines*) (*, $p < 0.05$). **b** Kaplan–Meier curve for recurrence-free survival after RFA therapy. The patients with high frequency of MDSCs (*solid line*) relapsed

concentrations of IL-1ra, IL-2, IL-6, IL-12(p70), and G-CSF tended to be increased in the group with high frequency of MDSCs. In accordance with our results, various cytokines, including IL-6, IL-10, IL-13, G-CSF, and VEGF, that trigger Janus kinase (JAK)-signal transducer and activator of transcription (STAT) signaling pathways have been reported to be associated with the frequency of MDSCs [39]. In particular, the cytokines involved in the JAK2-STAT3 signaling pathway are considered to be the main regulators of the expansion of MDSCs, which leads to stimulation of myelopoiesis and inhibition of myeloid-cell differentiation [40–42].